Exact method for the simulation of Coulombic systems by spherically truncated, pairwise r^{-1} summation

D. Wolf,[a] P. Keblinski, S. R. Phillpot, and J. Eggebrecht
Materials Science Division, Argonne National Laboratory, Argonne, Illinois 60439

(Received 9 July 1998; accepted 5 February 1999)

Based on a recent result showing that the net Coulomb potential in condensed ionic systems is rather short ranged, an exact and physically transparent method permitting the evaluation of the Coulomb potential by direct summation over the r^{-1} Coulomb pair potential is presented. The key observation is that the problems encountered in determining the Coulomb energy by pairwise, spherically truncated r^{-1} summation are a direct consequence of the fact that the system summed over is practically never neutral. A simple method is developed that achieves charge neutralization wherever the r^{-1} pair potential is truncated. This enables the extraction of the Coulomb energy, forces, and stresses from a spherically truncated, usually charged environment in a manner that is independent of the grouping of the pair terms. The close connection of our approach with the Ewald method is demonstrated and exploited, providing an efficient method for the simulation of even highly disordered ionic systems by direct, pairwise r^{-1} summation with spherical truncation at rather short range, i.e., a method which fully exploits the short-ranged nature of the interactions in ionic systems. The method is validated by simulations of crystals, liquids, and interfacial systems, such as free surfaces and grain boundaries. © *1999 American Institute of Physics.*
[S0021-9606(99)51517-1]

I. INTRODUCTION

The classic Madelung problem,[1] i.e., the problem of evaluating the Coulomb potential of condensed systems by direct, pairwise r^{-1} summation, and its consequences for the physics of ionic crystals and liquids, have received considerable attention throughout this century. The well-known Ewald method[2] has long been the method of choice for evaluating energies, forces, and stresses in the simulation of ionic liquids and solids. The method is based on a mathematical manipulation of the total Coulomb energy of a set of N ions, with charges q_i at positions $\mathbf{r}_i$ that are part of an infinite system of point charges,

$$E^{\text{tot}}=\frac{1}{2}\sum_{i=1}^{N}\sum_{j\neq i=1}^{\infty}\frac{q_iq_j}{r_{ij}}, \tag{1.1}$$

to achieve rapid convergence for what is mathematically a conditionally convergent expression; here $\mathbf{r}_{ij}=\mathbf{r}_j-\mathbf{r}_i$ and $r_{ij}=|\mathbf{r}_{ij}|$. The ''trick'' to the method consists of (i) artificially imposing structural periodicity on the generally aperiodic system, (ii) multiplying the resulting expression by unity, thus rewriting Eq. (1.1) as

$$E^{\text{tot}}=\frac{1}{2}\sum_{i=1}^{N}\sum_{j=1}^{N}\sum_{\mathbf{n}=\mathbf{0}}^{\infty}{}'\frac{q_iq_j}{|\mathbf{r}_{ij}+\mathbf{n}L|}[\text{erfc}(\alpha|\mathbf{r}_{ij}+\mathbf{n}L|)+\text{erf}(\alpha|\mathbf{r}_{ij}+\mathbf{n}L|)], \tag{1.2}$$

and (iii) taking the Fourier transform of only the error-function expression,

$$\text{erf}(\alpha r)=\frac{2}{\pi^{1/2}}\int_0^{\alpha r}\exp(-t^2)dt, \tag{1.3}$$

[with erf(0)=0 and erf(∞)=1] but not of the complementary error-function term,

$$\text{erfc}(\alpha r)=1-\text{erf}(\alpha r). \tag{1.4}$$

The vector $\mathbf{n}=(n_x,n_y,n_z)$ in Eq. (1.2) denotes the three-dimensionally (3D) periodic images of the simulation cell of linear size L; the prime indicates that, obviously, $\mathbf{n}\neq\mathbf{0}$ for $i=j$. The conditionally convergent total energy of the aperiodic system in Eq. (1.1) has thus been converted, by a few mathematical tricks, into the sum of rapidly converging real-space and reciprocal-space contributions,

$$E^{\text{tot}}=E_{\mathbf{r}}^{\text{tot}}+E_{\mathbf{k}}^{\text{tot}}, \tag{1.5}$$

of the artificially periodic system. Here $\mathbf{k}$ represents the reciprocal-lattice vectors associated with the 3D periodic simulation cell.

As a physicist one cannot help but think that the above mathematical procedure, converting a problem with no transparent *physical* solution into a straightforward *mathematical* exercise, is a scientific form of ''black magic.'' At the very least, one would like to (i) understand the physical implications of these manipulations and, even more important, (ii) expose the overall range of the *total* potential experienced by the ions, given that the r^{-1} *pair* potential is, indeed, very long ranged. Addressing these issues is the main purpose of this article.

From a conceptual viewpoint, the aperiodic nature of the original system should, in principle, be restored as the limit in which the reciprocal lattice vectors, $\mathbf{k}$, tend toward zero.

[a]Electronic mail: wolf@anl.gov

In practice, however, the reciprocal-space term, which accounts for long-range effects in the Coulomb potential, is usually retained. This has given rise to the popular notion of the long-ranged nature of the Coulomb potential in condensed ionic systems, and to the attribution of some ''typically ionic'' phenomena, such as the long-range charge ordering in ionic liquids,[3] to the long-range nature of the Coulomb pair potential.

There is much evidence, however, both theoretical[4] and from computer simulations,[5,6] that the effective Coulomb interactions in condensed systems are actually rather short ranged. For example, the direct-summation method devised by Evjen,[4] in which fractional charges are assigned to the ions according to their site symmetry, strongly suggests an effectively short-ranged nature of the Coulomb potential in the perfect crystal. Computer simulations of ionic melts have also contributed significantly to the growing body of evidence that at long range there is almost complete cancellation of Coulombic effects.[5,6] In fact, it has been demonstrated[5] that in practice the reciprocal-space part of the Ewald sum can be neglected entirely without affecting the underlying physics, leading Clarke *et al.*[5] to develop ''short-range effective'' potentials for the simulation of ionic liquids. Clearly, if the potential in Eq. (1.5) is therefore rather short ranged and essentially given by only the real-space part [see also Eq. (1.2)], the original potential in Eq. (1.1) must also be rather short ranged and, paradoxically, essentially identical to the real-space part of the Ewald sum. However, it is far from obvious how this can be. To elucidate this apparent paradox is one of the purposes of this article.

A key driving force for finding alternatives to the Ewald method is its high computational load, which in a simple implementation increases as $O(N^2)$. Moreover, even with an optimal balance of the real-space and reciprocal-space contributions Fincham[7] has shown that the computational load increases at best as $O(N^{3/2})$. Therefore, in recent years summation algorithms known as fast-multiple methods that are computationally superior to the Ewald method have become available for the simulation of Coulombic systems.[8–10] Based on the summation of the multipole expansion of Eq. (1.1), these order-N methods are particularly suited for the simulation of very large systems. In addition to their computational efficiency, these methods have the conceptual advantage over the Ewald sum of being more directly connected with the physics of ionic systems. Unfortunately, however, like the Ewald method they provide little physical insight into the effective range of the Coulomb potential and are therefore of little help in elucidating the physics of ionic systems from a more intuitive point of view.

That the effective Coulombic potential of the ions in condensed systems is actually rather short ranged was demonstrated more recently by Wolf.[11,12] By presenting a method for the evaluation of the Madelung constant for perfect crystals that involves direct r^{-1} lattice summation over neutral dipolar ''molecules,'' Wolf showed that the ''true'' Madelung potential of an ion due to its pairwise r^{-1} interaction with all the other ions falls off as r^{-5}.[11] Based on this insight and as a test of his method, he suggested that most ionic-crystal surfaces should be systematically reconstructed, particularly surfaces on charged crystal-lattice planes, an assertion tested by simulations of rocksalt structured surfaces[11,12] and later verified experimentally.[13]

In this article we will revisit the classic Coulomb problem, starting from an analysis of the physical reasons for the problems encountered when attempting to evaluate the Coulomb potential of condensed systems by simple, pairwise r^{-1} summation (Sec. II). The key recognition from this analysis is that the lack of electroneutrality prevents the pairwise, direct $1/r$ sum in Eq. (1.1) over spherical crystal-lattice shells from converging. In Sec. III a simple method is developed to achieve charge neutralization wherever the r^{-1} pair potential is spherically truncated, enabling the extraction of the Coulomb energy, forces, and stresses from a usually charged environment. The correspondence between the charge-neutralized and the shifted Coulomb pair potential is established, leading to a general method for smoothly shifting any interatomic potential and its derivatives in a manner that yields values for the energy, forces, etc. as close as desired to the correct (unshifted) ones. While a number of empirical approaches involving charge neutralization have been tried in the past,[5,14,15] here we develop a firm theoretical basis for the concept.

The concept of local charge neutrality leads naturally to a distinction between the true Madelung potential[16] and, as a part of it, the ''charge-neutralizing'' potential associated with the spherically truncated environment of each ion (Sec. III). By definition, the Madelung potential is unique in that it is entirely independent of the embedding of each ion in its local environment; it can be compared directly to that obtained from the Ewald sum. Plotted against the truncation radius, this potential is found to oscillate systematically, in a damped manner, about its fully converged value (Sec. IV), suggesting that the ''bare'' r^{-1} Coulomb *pair* potential can be replaced by a damped pair potential without significantly affecting the converged value of the Madelung potential. By justifying and carefully investigating the effects of damping, the close connection of our approach with the Ewald method is demonstrated (Secs. V and VI). This leads to a simple physical interpretation of the Ewald sum. Finally, to validate our method directly, in Sec. VII we compare molecular-dynamics simulations using direct, pairwise damped r^{-1} summation with spherical truncation with the results obtained via the full Ewald sum.

II. BACKGROUND

A. Charge neutrality and direct r^{-1} summation

The well-known problems encountered when attempting to determine the Coulomb energy by direct, pairwise r^{-1} summation over *crystal-lattice* shells out to some distance R_c are illustrated in Fig. 1 for the simple case of a rocksalt-structured perfect crystal at zero temperature.[12] Shown in Fig. 1(a) is the energy, $E_i^{\mathrm{tot}}(R_c)$, of removing some arbitrary ion, i, from the perfect crystal. $E_i^{\mathrm{tot}}(R_c)$ is related to the total energy of the system as follows [see Eq. (1.1)]:

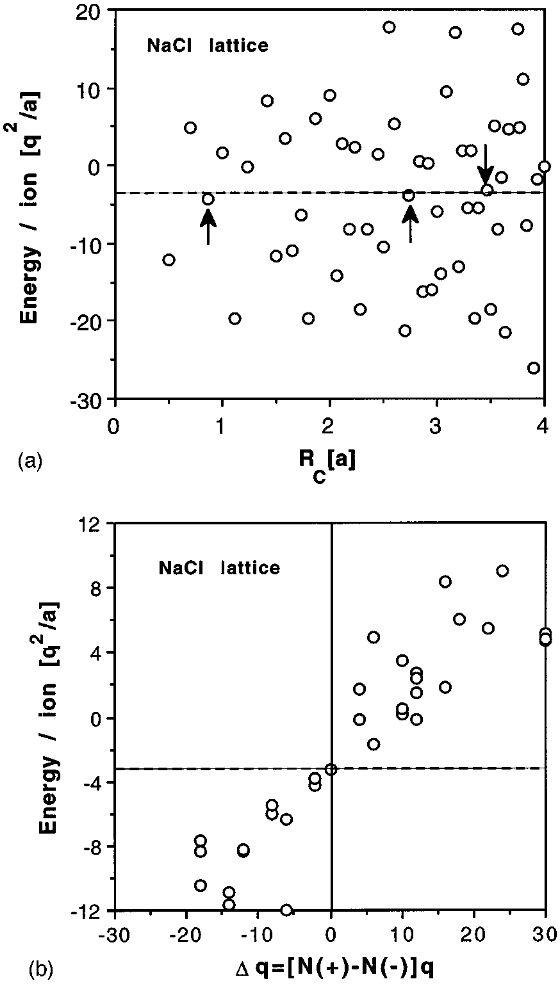

FIG. 1. Total Coulomb energy per ion (in units of the inverse lattice parameter, q^2/a) obtained by simply summing the Coulomb pair potential, $\pm q^2 r^{-1}$, over shells of the rocksalt lattice. (a) Energy per ion against cutoff radius, R_c, assumed to coincide with crystal-lattice shells; the arrows indicate cutoff radii where the crystal lattice is exactly or nearly neutral (b) energy per ion against the difference, $N(+)-N(-)$, between the total number of cations and anions contained in a crystal-lattice sphere of radius r. The fully converged value ($R_c\to\infty$) of the Madelung energy for this structure is indicated by the dashed line.

$$E^{\mathrm{tot}}(R_c)=\frac{N}{2}\sum_{\substack{j\neq i\\(r_{ij}<R_c)}}\frac{q_iq_j}{r_{ij}}=\frac{N}{2}E_i^{\mathrm{tot}}(R_c). \tag{2.1}$$

According to Fig. 1(a), the energy per ion thus defined fluctuates dramatically between large positive and negative values, with no indication of convergence towards the correct Madelung energy, $E^{\mathrm{Mad}}=-3.495\,129q^2/a$, for rocksalt[4] (dashed line). (We note that this value, given in units of the lattice parameter, is twice that given in units of the nearest-neighbor distance, $a/2$, for the NaCl lattice.[4]) With a value largely determined by the terminating crystal shell at R_c, from Fig. 1(a) it appears impossible to determine even the sign of the Madelung energy, irrespective of the volume of the system contained by the surface at R_c. This behavior illustrates the conditional convergence of the sum in Eq. (1.1), i.e., that the value of the Coulomb energy depends on the manner in which the sum in Eq. (1.1) is terminated and on the order in which the terms are grouped.

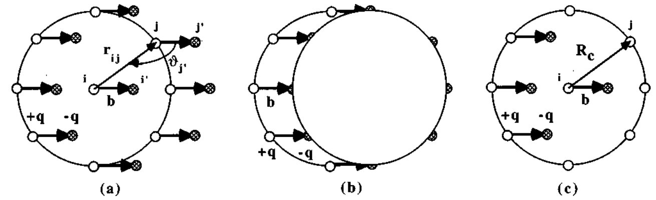

FIG. 2. (a) Neutral shells of NaCl molecules are obtained by attachment of the Na^+Cl^- basis dipoles to the sites of the fcc *Bravais lattice* (schematic; open and closed circles denote Na^+ and Cl^- ions, respectively). As illustrated in (b), this results in the generation of two identical, oppositely charged fcc sublattices that are displaced relative to each other by the basis vector **b**. (c) Spherical truncation of *crystal-lattice* shells usually results in a charged local environment of the ion at the center.

Figure 1(b), showing the energies of Fig. 1(a) plotted against the net charge, $\Delta q(R_c)$, in the spherical volume between $r=0$ and $r=R_c$, gives some indication as to the origin of this behavior.[12] Clearly, the deviations from the correct Madelung energy (dashed line) are approximately proportional to $\Delta q(R_c)$, suggesting that a reasonably good value of E_{Mad} could be obtained if one could find a way to render the volume summed over neutral. Indeed, when the system is neutral or almost neutral, values close to the correct Madelung energy are obtained [see the arrows in Fig. 1(a) corresponding to cutoff radii, R_c/a, of 0.866, 2.739, and 3.464 and values of $\Delta q(R_c)/|q|$ of -2, -2, and 0, respectively]. These observations suggest that the large fluctuations in Fig. 1(a) arise from the fact that the NaCl lattice is practically never neutral when terminated by complete crystal shells.

B. Short-ranged nature of the Madelung potential in a perfect ionic crystal

Based on the idea of charge neutralization, a simple method for determining the Madelung constant of a perfect crystal lattice was presented recently by Wolf.[11] As illustrated in Fig. 2(a), this approach involves a r^{-1} sum over the neutral shells of the *Bravais* lattice, with the proviso that no basis molecule may be broken up and thus guarantee charge neutrality wherever the r^{-1} pair potential is truncated; by contrast, the sum sketched in Fig. 2(c) involves the charged shells of the *crystal* lattice. For example, the rocksalt structure consists of a face-centered-cubic (fcc) Bravais lattice (open circles in Fig. 2) and a dipolar Na^+Cl^- basis molecule; the latter is characterized by the basis vector **b**. As illustrated in Figs. 2(a) and 2(b), this results in the generation of two identical, oppositely charged fcc sublattices that are displaced relative to each other by the vector **b**. The total ''molecular'' Coulomb energy of some ion i at the origin is then given by[11]

$$\begin{aligned}E_i^{\mathrm{mol}}&=-\frac{q^2}{b}+q^2\sum_{j\neq i=1}^{N/2}\sum_{j'=1}^{2}\left(\frac{1}{r_{ij}}-\frac{1}{r_{ij'}}\right)\\&=E_i^{\mathrm{intra}}+\sum_{r_s}E_i^{\mathrm{inter}}(r_s),\end{aligned} \tag{2.2}$$

where the first term represents the ''intramolecular'' (i

$-i'$) interaction while the second is the ''intermolecular'' interaction of ion i with the molecules in shells with radii $r_{ij} \equiv r_s$ [see Fig. 2(a)].

Intuitively one would expect the double sum in Eq. (2.2) (involving first all the Bravais sites and then the Na^+Cl^- basis molecules attached to each site) to converge rapidly for the following three reasons [see Fig. 2(a)]. First, the interaction energy of ion i with a complete molecule, $q^2/r_{ij} - q^2/r_{ij'}$, is small compared to its interaction energy with each individual ion in the molecule. Second, because the direction of $\mathbf{b}$ is fixed while that of $\mathbf{r}_{ij}$ is averaged over a discrete set of Bravais points on a sphere [see Fig. 2(a)], within a given Bravais-lattice shell of fixed radius r_s the values of $1/r_{ij} - 1/r_{ij'}$ vary between small positive and negative because the angle $\vartheta_{j'}$ between $\mathbf{r}_{ij}$ and $\mathbf{b}$ is symmetrically distributed; the sum over j in Eq. (2.2), involving all the molecules in a given Bravais shell, therefore involves differences between already relatively small terms. Third, the very small positive and negative shell-by-shell values, $E_{\mathrm{inter}}(r_s)$, thus obtained are further averaged while being summed over all Bravais shells; as r_s increases, these rapidly decreasing small negative and positive values thus effectively average to zero.

While this dipolar approach guarantees that the crystal lattice is neutral irrespective of where the pairwise sum is truncated, it suffers from the problem that a sum over shells of dipoles cannot be terminated without rendering the system as a whole polarized [see Fig. 2(b)]. To obtain the correct Madelung energy, the polarization energy per unit volume, E^{pol}, therefore has to be subtracted from the expression in Eq. (2.2), i.e.,

$$E_i^{\mathrm{Mad}} = E_i^{\mathrm{mol}} - E^{\mathrm{pol}}. \tag{2.3}$$

According to de Leeuw *et al.*,[15] E_{pol} is given by the dipole moment, $q\mathbf{b}$, that each molecule contributes to the polarization of the system, $E^{\mathrm{pol}} = (2\pi/3\Omega)(qb)^2$, where Ω is the ''molecular'' volume. For example, in the fcc lattice, $\Omega = a^3/4$; with $|\mathbf{b}| = a/2$ for the Na^+Cl^- basis molecule, this expression gives $E^{\mathrm{pol}} = (2\pi/3)q^2/a = 2.094\,39/a$.

By choosing a basis molecule without a dipole moment, the polarization correction in Eq. (2.3) can be avoided altogether. Thus, instead of viewing the NaCl lattice as a fcc Bravais lattice with a *dipolar* basis, one can choose the simple cubic (sc) Bravais lattice with a cube-shaped *octopolar* $(NaCl)_4$ basis.[11] Avoiding thus the generation of a macroscopic polarization, the direct r^{-1} sum based on Eq. (2.2) gives the correct Madelung energy directly, without any correction. The results of the evaluation of Eqs. (2.2) and (2.3) for a ''molecular'' rocksalt lattice viewed in either of these two ways (fcc versus sc Bravais lattice, dipolar versus octopolar basis) are summarized in Fig. 3.

A formal investigation of the convergence behavior of E_i^{mol} in Eqs. (2.2) and (2.3) with Figs. 2(a) and 2(b) was presented in Ref. 11, showing that E_i^{mol} can be written as an expansion in powers of $(b/r_s)^{n+1}$ ($n = 4,6,8...$,). The leading term has the form[11]

$$E_i^{\mathrm{mol}} \approx \frac{7}{8}\frac{q^2}{b}\sum_{r_s} N(r_s)\left(\frac{b}{r_s}\right)^5 [1 - 5c_4(r_s)], \tag{2.4}$$

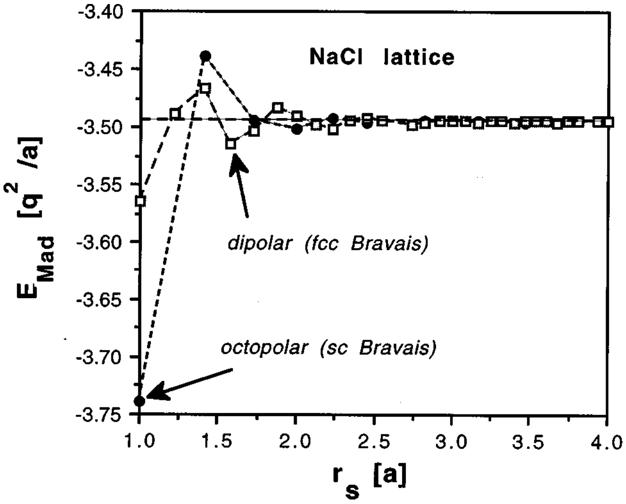

FIG. 3. Madelung energy for the NaCl lattice against cutoff radius obtained by direct lattice summation involving either a fcc Bravais lattice with a dipolar basis (open symbols) or a sc Bravais lattice with an octopolar basis (closed symbols). The horizontal line indicates the correct Madelung energy.

where $N(r_s)$ is the number of sites (i.e., Na^+Cl^- molecules) in a given Bravais shell, and $c_n(r_s) \equiv \langle \cos^n \vartheta \rangle r_s = [1/N(r_s)]\Sigma_{j'(r_s)} \cos^n \vartheta_{j'}$ represents an average performed over each Bravais shell [see also Fig. 2(a)]. Because of the inversion symmetry of Bravais lattices, all odd powers of $c_n(r_s)$ vanish identically.

We note that the coefficients in the expansion in powers of $(b/r_s)^{n+1}$ ($n = 4,6,8...$,) given in Ref. 11 are actually the Legendre polynomials, $P_n(x)$, of $x = c_n(r_s)$.[17] Moreover, from the addition theorem the Legendre polynomials may be written in terms of spherical harmonics.[17] It is precisely such an expansion of the electrostatic potential in terms of spherical harmonics that forms the basis for the fast-multipole methods.[8–10]

We also mention that for the case of the rocksalt structure the direct r^{-1} sum involving octopolar building blocks reproduces Evjen's sum[4] identically while avoiding the ambiguities associated with the assignment of fractional charges to the ions in the unit cell.[4] Also, based on the above insights it was predicted[11,18] that all rocksalt structured surfaces should be fundamentally reconstructed such that the octopolar building blocks are not broken up. One such reconstruction has indeed been recently observed,[13] and this strongly supports the validity of the physical picture underlying the above convergence analysis.

The effective range of E_i^{mol} in Eq. (2.4) may be estimated by determining how the error, $\Delta E^{\mathrm{Mad}}(R_c)$, due to the truncation varies as a function of R_c. This error is given by the interaction of ion i with all the ions beyond some cutoff radius, R_c:

$$\Delta E^{\mathrm{Mad}}(R_c) = \sum_{r_s > R_c} N(r_s) V_{\mathrm{eff}}(r_s) \approx \rho \int_{R_c}^{\infty} dr_s 4\pi r_s^2 V_{\mathrm{eff}}(r_s), \tag{2.5}$$

where the sum was converted into an integral and ρ is the number density; $V_{\mathrm{eff}}(r_s)$ represents the effective pair potential defined by comparison with Eq. (2.4). The shell-by-shell values of $c_4(r_s)$ scatter practically randomly about 0.2,[12] i.e., $1-5c_4(r_s)$ fluctuates about zero, giving rise to the practically random fluctuations about zero in the dipolar values for E_i^{mol} in Fig. 3. To obtain an upper bound for the envelope of these fluctuations, $1-5c_4(r_s)$ can be set equal to some constant; with $V_{\mathrm{eff}}(r_s)\sim r_s^{-5}$, the integral then yields a quadratic decrease, $\Delta E^{\mathrm{Mad}}(R_c)\sim R_c^{-2}$. For comparison, with $V_{\mathrm{eff}}(r)\sim r^{-6}$, the Lennard-Jones potential gives $\Delta E(R_c)\sim R_c^{-3}$.

C. Convergence behavior for disordered systems

That the above convergence arguments are not limited to perfect crystal lattices nor even solids is readily seen. Most computer simulations of solids and liquids make use of artificially imposed 3D periodic cell borders, particularly when evaluating the Coulomb energy and forces via the Ewald method. A simple way of mapping a liquid onto the above molecular way of thinking, for example, is to consider *the entire simulation cell* as the neutral ''molecule'' attached to the sc lattice of the periodic simulation-cell images. At any instant the simulation cell will exhibit some small net dipole moment, enabling a power expansion mathematically identical to that in Eq. (2.4). Even in a liquid the r^{-5} convergence therefore results.

Apart from this convergence argument, in practice the simulation of a highly disordered ionic system in the spirit of the above molecular, direct r^{-1} sum is not trivial and is computationally rather inefficient. It necessitates some artificial and computationally cumbersome grouping of the ions into molecules, combined with a method for truncating the r^{-1} pair potential. In one implementation of this approach for the molecular-dynamics simulation of ionic melts,[19] truncation of the pair potential was avoided altogether by summing to full convergence. These simulations exhibited energy conservation and gave thermal properties in full agreement with similar simulations using the Ewald sum.[19] Nevertheless, a more practical approach is clearly needed. Such an approach should combine the conceptual advances associated with recognizing the short-ranged nature of the effective Coulomb potential of the ions with a computationally efficient and physically transparent method for truncating the r^{-1} pair potential.

III. PAIRWISE, SPHERICALLY TRUNCATED r^{-1} SUM

The present situation, described in Secs. I and II, can be summarized by the following four observations. First, Fig. 1(a) demonstrates the well-known fact that the total Coulomb energy of a given system obtained by evaluating Eq. (1.1) depends entirely on the manner in which the ions are surrounded for the purpose of evaluating the pairwise r^{-1} double sum.

Second, the ''molecular'' approach reviewed in Secs. II B and II C reveals that the true Madelung potential of the ions is rather short ranged even in a highly disordered solid or in liquids. However, in order to recognize this property, the pairwise r^{-1} double sum in Eq. (1.1) has to be performed in such a manner as to ensure a neutral local environment for each ion.

Third, the slow rate of decay of the r^{-1} Coulomb pair potential has to be distinguished from the fast rate of convergence of the Madelung energy as a function of the cutoff radius, R_c.

Fourth, largely due to the reciprocal-space term, the range of the net Coulomb potential obtained from the Ewald sum is not clear. Although in the Ewald method little attention is paid to the manner in which the ions are surrounded, its numerical robustness suggests that the underlying potential is also rather short ranged.

How these four observations are connected is not obvious, as evidenced by a considerable body of literature that has dealt with the Coulomb problem in condensed systems throughout this century. It is the main purpose of this article to elucidate these connections.

A. Madelung potential of a perfect crystal from spherical truncation

We start by considering the two *finite* perfect-crystal systems sketched in Figs. 2(a) and 2(c). To understand the difference between the energy of ion *i* at the center of Fig. 2(c), on the one hand, and at the center of Fig. 2(a), on the other, we observe that the charged system in Fig. 2(c) represents merely a spherically truncated subset contained in the neutral system in Fig. 2(a) which has been truncated in a nonspherical manner.[11] Since in both systems the energy of ion *i* at the center consists of a *finite* number of pairwise r^{-1} terms [see, e.g., Eq. (2.1)], their energy difference can be determined from a one-by-one comparison of corresponding pair terms. Inspection of Figs. 2(a) and 2(c) reveals that the key difference between the two systems is due to the net charge, $\Delta q_i(R_c)$, in the system in Fig. 2(c) that arises from those Na^+Cl^- dipoles in Fig. 2(a) that were broken up upon spherical truncation at R_c. The entire net charge in Fig. 2(c) is therefore localized near the system surface, in a shell of width $|\mathbf{b}|$, while the interiors of both systems are identical and neutral.

By analogy with the convergent behavior of the charge-neutralized system in Fig. 2(a), one might expect that the system in Fig. 2(c) might become convergent as well if only the charge-neutralizing potential associated with the net system charge is subtracted from the total energy [see also Sec. II A and Fig. 1(b)], i.e.,

$$E_i^{\mathrm{Mad}}(R_c)\approx E_i^{\mathrm{tot}}(R_c)-E_i^{\mathrm{neutr}}(R_c), \tag{3.1}$$

with $E_i^{\mathrm{tot}}(R_c)$ defined in Eq. (2.1).

Based on the insight that the net charge in the system in Fig. 2(c) is localized near the system surface, a simple model can be developed to estimate its effect on ion *i* at the center. Given that $|\mathbf{b}|$ represents the nearest-neighbor distance, $|\mathbf{b}|/R_c$ is always less than unity and, for longer cutoff radii, $|\mathbf{b}|/R_c\ll 1$. Instead of considering the actual charge distribution within the thin surface shell of thickness $|\mathbf{b}|$, we therefore assume that the entire net charge is located *exactly at* the system surface at R_c. The charge-neutralizing potential for ion *i* in Fig. 2(c) is then simply given by its Coulomb interaction with the surface charge, $\Delta q_i(R_c)$, i.e.,

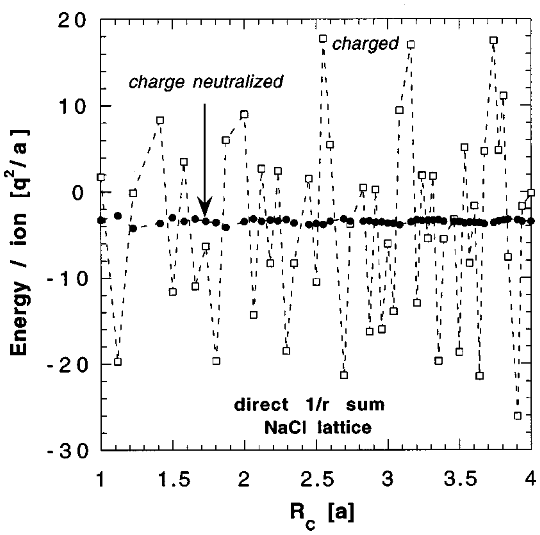

FIG. 4. R_c dependence of the approximate Madelung energy determined from Eq. (3.3) for the spherically truncated, charge-neutralized system in Fig. 2(c) (closed symbols). For comparison, the total energy of the charged system [first term in Eq. (3.3)] is also shown [open squares; same data as in Fig. 1(a)].

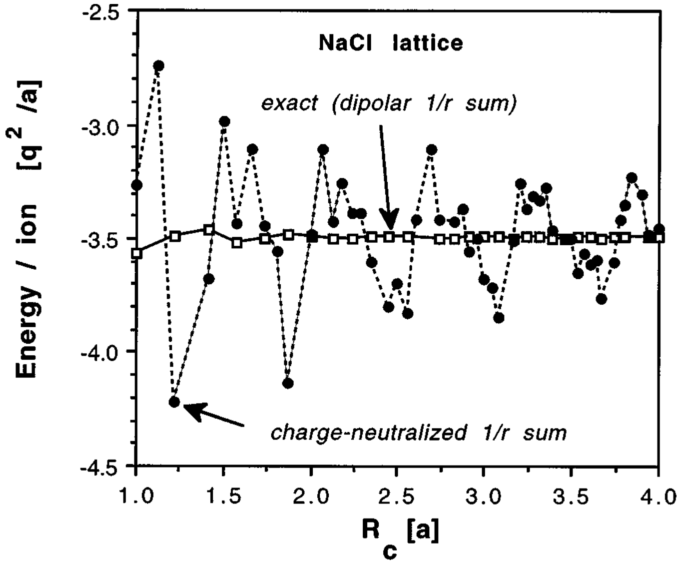

FIG. 5. Comparison of the approximate Madelung energies against R_c obtained from Eq. (3.3) (closed symbols; see also Fig. 4) with the exact ones from Fig. 3 (open squares).

$$E_i^{\mathrm{neutr}}(R_c) \approx \frac{q_i \Delta q_i(R_c)}{R_c}, \tag{3.2}$$

where $\Delta q_i(R_c) = q(N^+ - N^-)$ is the net charge within the cutoff sphere of ion *i*. We note that in the particular case considered in Figs. 2(a) and 2(c), $N^+ > N^-$ and hence $E_i^{\mathrm{neutr}} > 0$. Combining Eqs. (3.2), (3.1), and (2.1), we obtain

$$E_i^{\mathrm{Mad}}(R_c) \approx \sum_{\substack{j \neq i \\ (r_{ij} < R_c)}} \frac{q_i q_j}{r_{ij}} - \frac{q_i \Delta q_i(R_c)}{R_c}. \tag{3.3}$$

The dramatic effect of this charge neutralization on the energy of the spherically truncated system is demonstrated in Fig. 4 in which the energy of the charge-neutralized systems is compared with that of the charged system in Fig. 1(a). Remarkably, even for rather short cutoff radii, Madelung energies close to the correct value for rocksalt are obtained (solid symbols).

Equation (3.3) is a remarkable result, demonstrating that the Madelung energy of an ion in a charged environment [see Fig. 2(c)] can be estimated by simply subtracting the charge-neutralization term from the energy of the charged system. However, as seen from the detailed comparison in Fig. 5, the approximate Madelung energy obtained from Eq. (3.3) (solid symbols; see also Fig. 4) oscillates significantly, in a slightly damped manner, about the correct Madelung energy of the dipolar molecular system (open symbols in Figs. 5 and 3); in fact, on the greatly expanded scale in Fig. 5, the small oscillations in the potential of the dipolar system are barely discernible (cf. Fig. 3).

In an attempt to analyze the origin of the pronounced oscillations in the charge-neutralized, spherically truncated potential in Fig. 5, we have determined the charge density in each crystal shell, defined by dividing the charge and energy stored in each shell by its volume, $4\pi R_c^2 \Delta d$, where Δd is the distance to the next shell. As seen from Fig. 6, these *shell-by-shell* charge densities (open symbols, right-hand axis) exhibit basically the same short-period fluctuations as the total energy of the charged system in Figs. 1(a) and 4. As also shown in Fig. 6 (left-hand axis), the *total* charge density of the system, defined by dividing the total charge of the entire system by its total volume, $4\pi R_c^3/3$, exhibits the same noisy behavior. We therefore conclude that the charge stored in each crystal shell, or in the system as a whole out to R_c, is *not* responsible for the damped oscillations in the charge-neutralized, spherically truncated potential in Fig. 5. The origin of these oscillations will be elucidated in Sec. IV.

In summary, based on the insight that any net charge contained in a spherically truncated perfect crystal [Fig. 2(c)] is localized near the system surface while the interior is neutral, we were able to demonstrate that the Madelung energy of an ion in a spherically truncated environment [Fig. 2(c)]

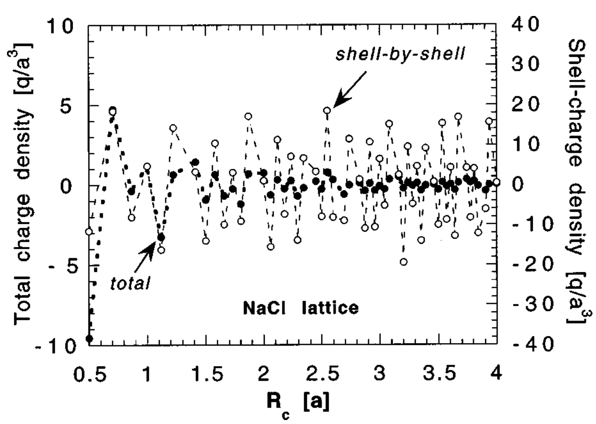

FIG. 6. Charge density in each crystal shell, defined by dividing the charge in the shell by its volume, $4\pi R_c^2 \Delta d$, where Δd is the distance to the next shell (open symbols; right-hand axis). Also shown is the integrated charge density (closed symbols; left-hand axis), defined by dividing the total charge in the entire system by its total volume, $4\pi R_c^3/3$.

can be estimated by simply subtracting a surface-charge term from the total energy of the charged system.

We also mention that Adams[14] has pointed out that, operationally, an electroneutrality correction identical to Eq. (3.2) involving a charge distribution opposite to the total net charge in the truncation sphere of each ion removes the major deficiency of the direct summation over the Coulomb pair potential. In the absence of either a formal justification or a convergence argument, Adams' operational suggestion has gone mostly unnoticed. Unfortunately, however, his simulations at the time of relatively small systems led him to conclude that the results thus obtained are strongly system-size dependent, which we were not able to confirm. Nevertheless, in a 512 ion Monte-Carlo simulation of a molten salt he was able to approximately reproduce the radial distribution function obtained from the Ewald method.[14]

We finally point out that, as an extra benefit, the spherical truncation of the system in Fig. 2(a) has eliminated the net dipole moment in the system [see Fig. 2(b)] and, hence, the related dipolar correction given by Eq. (2.3), i.e., as a natural consequence of spherical truncation, the local environment of each ion is neutral[20] *and* dipole free.

B. Madelung potential for disordered systems from spherical truncation

The above results, derived for a highly idealized perfect-crystal situation, are readily generalized to include disordered systems, such as liquids or solids with defects. Our main conclusion will be that the approximation in Eq. (3.2) that any net charge in a spherically truncated system is located *exactly at* the surface rather than distributed over a discrete surface shell of width $|\mathbf{b}|$ is actually much better satisfied in highly disordered systems.

In a disordered system the energy and forces vary from ion to ion, as does the net charge, $\Delta q_i(R_c)$, within the cutoff sphere of each ion. The double sum in the perfect-crystal expression (2.1) therefore has to be restored [see also Eq. (1.1)]:

$$E^{\mathrm{tot}}(R_c)=\frac{1}{2}\sum_{i=1}^{N}\sum_{\substack{j\neq i\\(r_{ij}<R_c)}}\frac{q_iq_j}{r_{ij}}=\frac{1}{2}\sum_{i=1}^{N}E_i^{\mathrm{tot}}(R_c). \tag{3.4}$$

Instead of the perfect crystal sketched in Figs. 2(a) and 2(c) one might think of a liquid, considered in Fig. 2(a) as a neutral, ''molecular'' system with the r^{-5} convergence behavior discussed in Sec. II B, and in Fig. 2(c) as a spherically truncated system. Since in their interiors the two systems are identical and neutral, any net charge in the spherically truncated liquid arises from molecules near the surface that were broken up upon spherical truncation of the neutral, molecular system, and Eqs. (3.2) and (3.3) are replaced by

$$E_{\mathrm{tot}}^{\mathrm{neutr}}(R_c)\approx\frac{1}{2}\sum_{i=1}^{N}E_i^{\mathrm{neutr}}(R_c)\approx\frac{1}{2}\sum_{i=1}^{N}\frac{q_i\Delta q_i(R_c)}{R_c}, \tag{3.5}$$

and

$$E_{\mathrm{tot}}^{\mathrm{Mad}}(R_c)\approx\frac{1}{2}\sum_{i=1}^{N}E_i^{\mathrm{Mad}}(R_c)\approx\frac{1}{2}\sum_{i=1}^{N}\left(\sum_{\substack{j\neq i\\(r_{ij}<R_c)}}\frac{q_iq_j}{r_{ij}}-\frac{q_i\Delta q_i(R_c)}{R_c}\right). \tag{3.6}$$

This general expression suggests that the total Madelung energy, $E_{\mathrm{tot}}^{\mathrm{Mad}}(R_c)$, of an arbitrarily disordered, spherically truncated, charged system can be estimated simply by subtracting the charge-neutralization term associated with the local environment of each ion from the total energy of the charged system.

As an illustration of Eq. (3.6), in the following we consider crystalline and molten MgO as described by the Buckingham-type interionic potentials of Sangster and Stoneham.[21] A melt was prepared by means of standard constant-pressure molecular-dynamics simulations of a point-ion model in which the Coulomb energy, forces, and stresses were evaluated using the full 3D Ewald method. During gradual heating of the crystal at constant (zero) pressure from zero temperature through the melting point, snapshots of the structures of the high-temperature crystal and the liquid were stored for the following analysis using Eq. (3.6).

The dramatic effects of charge neutralization are demonstrated in Fig. 7(a) for the high-temperature perfect crystal and in Fig. 7(b) for the melt. Shown in each is both the total energy per ion in the charged system and the charge-neutralized (Madelung) energy obtained from Eq. (3.6). Remarkably, for both systems Madelung energies close to the fully converged Ewald values [horizontal lines in Figs. 7(a) and 7(b)] are obtained even for rather short cutoff radii. Also, damping in the oscillations about the correct Madelung energy is clearly discernible in both cases.

As already mentioned, the assumption underlying Eq. (3.5) is that the net charge within the cutoff sphere of each ion is located *exactly at* the sphere surface rather than discretely distributed over a width of the order of the nearest-neighbor distance. The direct comparison in Fig. 8 of the approximate Madelung energies thus obtained for the zero- and high-temperature crystals and for the melt reveals that the magnitude of the damping in the oscillations about the correct Madelung energy increases with the increasing degree of structural disorder, indicating that this assumption is better satisfied the more disordered the system is. This behavior originates from the thermal movements of the ions which have the effect of smearing out the discrete distribution of the surface ions. The net effect is a smaller net charge within the truncation volume that has to be neutralized; also, while in the high-temperature crystal some of the directional and radial discreteness in this distribution remains, in the melt it is almost completely washed out.

In Fig. 9 the charge-neutralizing energies from Figs. 7(a) and 7(b) are compared directly; these energies are directly related to the surface charges in the spherically truncated system. Compared to the zero-temperature perfect-crystal data in Fig. 4, due to the ion mobility at higher temperatures the charge-neutralization energies for the high-temperature solid and the melt exhibit a rather smooth oscillatory depen-

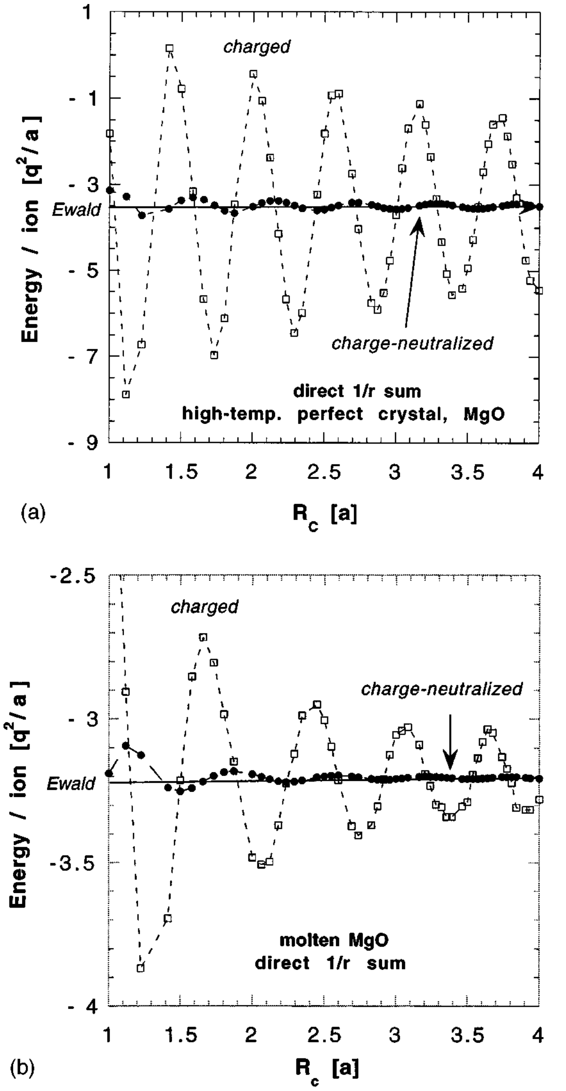

FIG. 7. Comparison between the charged and charge-neutralized energies of (a) the high-temperature perfect crystal and (b) the melt as a function of R_c. Both systems were prepared by constant-pressure molecular-dynamics simulations using the full Ewald sum.

dence on R_c, and with a greatly reduced magnitude. This oscillatory behavior arises from long-range charge ordering, as seen, for example, in the charge–charge correlation function.[6] It is interesting to note the slightly different frequencies of the charge oscillations in the melt and in the high-temperature crystal, suggesting qualitatively different charge-ordering effects in the two systems.[6]

In summary, the above results demonstrate that, even for highly disordered systems, the problems in evaluating the total energy in Eq. (3.4) by direct r^{-1} lattice summation with spherical truncation arise from the net charge in the system for some arbitrary value of R_c. Moreover, the oscillations in the total (non-neutralized) energy of a spherically truncated system at finite temperature appear to be a physical effect associated with charge ordering in the real system.

Finally, we consider two simple types of interfacial systems, namely, free surfaces and grain boundaries (GBs). Compared to the two, more or less homogeneously disordered *bulk* systems considered above, interfacial systems are

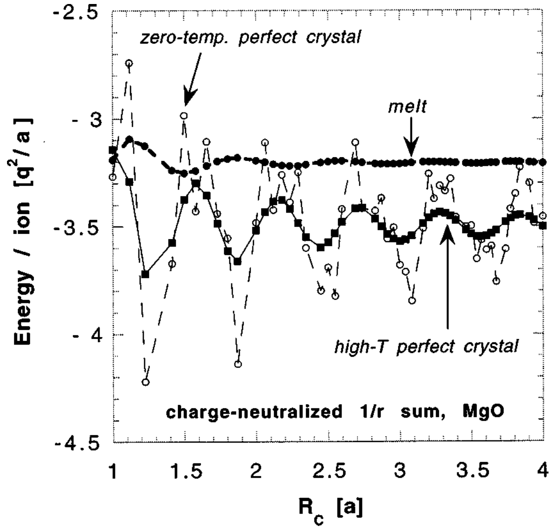

FIG. 8. Comparison of the charge-neutralized energies of the high-temperature perfect crystal and the melt [see Figs. 7(a) and 7(b)] with that of the zero-temperature perfect crystal in Fig. 5.

physically and computationally more complex because the structural disorder is so highly localized at the interfaces. The key task is to determine the Gibbsian excess energy per unit area from the simulation of two related systems, one a perfect-crystal reference system and the other a bicrystal containing the interface, but otherwise identical to the reference crystal (i.e., they contain the same number of ions, at the same temperature and pressure). The computational challenge is therefore to extract a relatively small (intensive) excess energy per unit area from the subtraction of two large (extensive) system energies.

For simplicity we limit ourselves to zero temperature. The two systems we choose are the (100) free surface of MgO and the symmetric tilt GB (STGB) on the MgO (210) plane; both systems were the subject of earlier investigations[22–24] involving static lattice relaxation and Parry's modification of the 3D Ewald sum[25] that permits con-

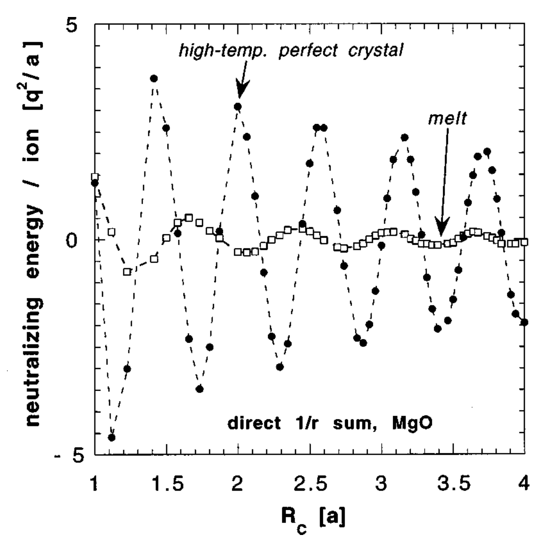

FIG. 9. Direct comparison of the surface-charge neutralization energies of Figs. 7(a) and 7(b).

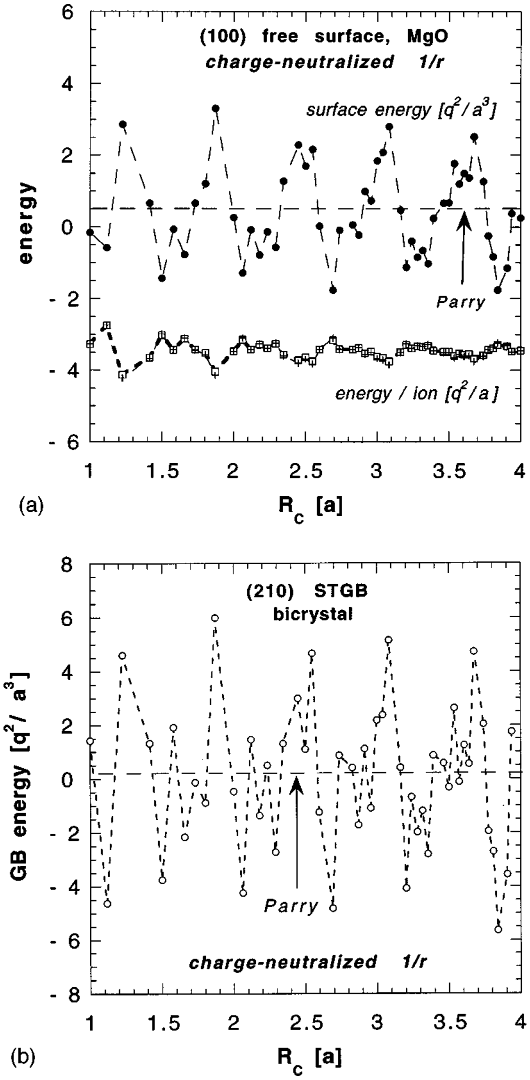

FIG. 10. Interface energy (i.e., Gibbsian excess energy per unit area) for (a) the (100) free surface and (b) the (210) symmetric tilt boundary in MgO (in units of q^2/a^3). To demonstrate the subtraction of two large numbers necessary to obtain these excess energies, in (a) the total Madelung energy per ion (in units of q^2/a) in the system containing the surface (squares) and the perfect-crystal reference system (crosses) are shown also. The dashed horizontal line indicates the interface energy obtained via Parry's slab version of the Ewald sum (Ref. 25).

sideration of a slab geometry. For our present purpose, their relaxed zero-temperature structures were determined by means of the potentials of Sangster and Stoneham[21] and a point-ion model in which the Coulomb energy, forces, and stresses were evaluated using Parry's slab method.[25] Using these as input structures, the charge-neutralized Coulomb energies were subsequently evaluated using Eq. (3.6).

To demonstrate the subtraction of two large, rather similar sets of energies to determine the interface energy, in the free-surface results in Fig. 10(a) we have included two distinct sets of data: first, the total Madelung energy per ion (in units of q^2/a) in the system containing the surface (squares) and the perfect-crystal reference system (crosses); second, the Coulombic contribution to the total Gibbsian excess energy per unit area (i.e., the interface energy) in units of q^2/a^3, obtained from the first set; by contrast, the GB results in Fig. 10(b) show only the interface energy.

The somewhat disappointing result in Figs. 10(a) and 10(b) is that the excess energy oscillates dramatically about the correct value obtained by means of Parry's formula (dashed horizontal line); in fact, in both cases we are unable to determine even the correct sign of the Coulombic contribution to the interface energy. This numerical, second-order effect arises from the fact that the underlying uncertainties in the Madelung energies per ion in the system are of roughly the same magnitude as the excess energy per ion in the interface. In Sec. V A we will show how the effects of damping imposed on the Coulomb pair potential enable realistic simulations of interfacial systems by direct lattice summation.

C. Shifted Coulomb pair potential

For the charge-neutralized Coulomb potential to be usable, for example, in lattice-statics or molecular-dynamics simulations, the relevant expressions for the forces and stresses must be derived from Eq. (3.6). Moreover, a method for shifting the potential and its derivatives has to be developed so as to avoid any discontinuities in the energy, forces, and stresses at the surface of the truncation sphere.

Prior to tackling these problems, however, we develop a more formal theoretical understanding of the charge-neutralization term in Eqs. (3.5) and (3.6). As is readily seen, the latter can be rewritten as follows:

$$E_{\mathrm{tot}}^{\mathrm{neutr}}(R_c) \approx \frac{1}{2}\sum_{i=1}^{N} \frac{q_i \Delta q_i(R_c)}{R_c} = \frac{1}{2}\sum_{i=1}^{N} \sum_{\substack{j=1 \\ (r_{ij}<R_c)}}^{N} \frac{q_i q_j}{R_c}, \tag{3.7}$$

because the net charge within the spherical truncation shell of any ion i is given by

$$\Delta q_i(R_c) = \sum_{\substack{j=1 \\ (r_{ij}<R_c)}}^{N} q_j . \tag{3.8}$$

We note that the term for $j=i$ needs to be included here so that the true total charge in the spherically truncated volume is obtained; the latter obviously includes the ion at the center of the truncation sphere. Inserting Eq. (3.7) into (3.6), we obtain

$$E_{\mathrm{tot}}^{\mathrm{Mad}}(R_c) = E^{\mathrm{tot}}(R_c) - E_{\mathrm{tot}}^{\mathrm{neutr}}(R_c)$$
$$\approx \frac{1}{2}\sum_{i=1}^{N} \sum_{\substack{j\neq i \\ (r_{ij}<R_c)}} \frac{q_i q_j}{r_{ij}} - \frac{1}{2}\sum_{i=1}^{N} \sum_{\substack{j=1 \\ (r_{ij}<R_c)}}^{N} \frac{q_i q_j}{R_c}, \tag{3.9}$$

or, more explicitly,

$$E_{\mathrm{tot}}^{\mathrm{Mad}}(R_c) = \frac{1}{2}\sum_{i=1}^{N} \sum_{\substack{j\neq i \\ (r_{ij}<R_c)}} V_{\mathrm{sh}}^{C}(r_{ij}) - \frac{1}{2R_c}\sum_{i=1}^{N} q_i^2, \tag{3.10}$$

where we have introduced the "shifted" Coulomb pair potential,

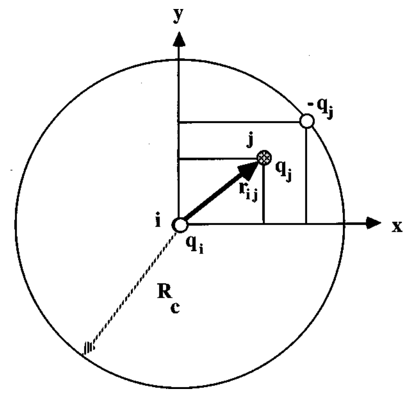

FIG. 11. An interpretation of Eqs. (3.10) and (3.11) is that for every charge q_j at distance r_{ij} from some central ion i, an image charge of opposite sign is projected onto the truncation sphere at R_c, such that ion i effectively interacts only with neutral pairs.

$$V_{\rm sh}^C(r_{ij})=q_iq_j\left(\frac{1}{r_{ij}}-\frac{1}{R_c}\right)\quad (r_{ij}<R_c),$$
$$V_{\rm sh}^C(r_{ij})=0\quad (r_{ij}>R_c). \tag{3.11}$$

This interesting result reveals that the physical concept of charge neutralization at the system surface and the operational concept of shifting of the pair potential are equivalent. As first pointed out by Adams,[14] the charge-neutralized energy of the spherically truncated system can therefore be written in terms of a shifted pair potential which smoothly approaches zero at $r=R_c$. The additive constant in Eq. (3.10), which involves a sum over the squares of the charges in the system, is a self term for each ion that is unaffected by the pair interactions between the ions and merely added to the total Madelung energy of the system.

In view of Eqs. (3.10) and (3.11), we propose the following interpretation of the manner in which the Madelung energy can be extracted from the total energy of the spherically truncated, charged system. For every charge q_j at distance r_{ij} from some central ion i, an image charge of opposite sign is projected onto the truncation sphere at R_c, such that ion i effectively interacts only with neutral pairs (see Fig. 11). The image-charge potential, $-q_iq_j/R_c$, is then added to the unshifted Coulomb potential, q_iq_j/r_{ij}, so as to achieve charge neutralization in the energy and all its derivatives; this results in a smooth truncation of the pair potential at R_c. As a consequence, the interactions of the central ion with the ions at R_c (which are responsible for the net charge in the system) and with the entire material beyond R_c vanish, thus effectively delineating a neutral, spherical environment for each ion from which its Madelung energy can be extracted.

As written, the neutralizing potential in Eqs. (3.7), (3.9), and (3.10) is a constant for any given value of R_c. Formally, the ions on the surface of the truncation sphere would therefore have no effect whatsoever on the forces and stresses on the ion at the center, a result that is unphysical. Clearly, the surface ions exert a (positive or negative) pressure on the system and give rise to forces, effects that must be taken into account.

A slight modification of Eq. (3.7) readily permits incorporation of these effects. By introducing the $r_{ij}\to R_c$ limit into Eq. (3.7), according to

$$E_{\rm tot}^{\rm neutr}\approx \lim_{r_{ij}\to R_c}\left\{\frac{1}{2}\sum_{i=1}^{N}\sum_{\substack{j\neq i\\(r_{ij}<R_c)}}\frac{q_iq_j}{r_{ij}}\right\}+\frac{1}{2R_c}\sum_{i=1}^{N}q_i^2, \tag{3.12}$$

and evaluating all derivatives *prior to* taking the limit, all effects due to the surface charge are fully incorporated while rendering the energy in Eq. (3.10) unchanged. The rationale for leaving the self term out of the limit is that an ion does not exert a force nor a pressure on itself; this constant term will thus not contribute to the derivatives of Eq. (3.12).

The shifted pair potential in Eq. (3.11) is hence replaced by

$$V_{\rm sh}^C(r_{ij})=\frac{q_iq_j}{r_{ij}}-\lim_{r_{ij}\to R_c}\left\{\frac{q_iq_j}{r_{ij}}\right\}, \tag{3.13}$$

while Eq. (3.10) remains formally unchanged. In analogy to Eq. (3.3) we define the Madelung energy of ion i as

$$E_i^{\rm Mad}(R_c)=\sum_{\substack{j\neq i\\(r_{ij}<R_c)}}V_{\rm sh}^C(r_{ij}). \tag{3.14}$$

The starting equation (3.10) for evaluating the forces and stresses may then be rewritten as follows:

$$E_{\rm tot}^{\rm Mad}(R_c)\approx\frac{1}{2}\sum_{i=1}^{N}E_i^{\rm Mad}(R_c)-\frac{1}{2R_c}\sum_{i=1}^{N}q_i^2. \tag{3.15}$$

The $\alpha(=x,y,z)$ component of the force on ion i is defined in the usual manner by

$$F_{i\alpha}(R_c)=-\frac{\partial E_i^{\rm Mad}}{\partial r_{i\alpha}}=-\frac{\partial}{\partial r_{i\alpha}}\left[\sum_{\substack{j\neq i\\(r_{ij}<R_c)}}V_{\rm sh}^C(r_{ij})\right]$$
$$=-\sum_{\substack{j\neq i\\(r_{ij}<R_c)}}\frac{dV_{\rm sh}^C(r_{ij})}{dr_{ij}}\frac{\partial r_{ij}}{\partial r_{i\alpha}}. \tag{3.16}$$

With [see Eq. (3.13)]

$$\frac{dV_{\rm sh}^C(r_{ij})}{dr_{ij}}=-q_iq_j\left(\frac{1}{r_{ij}^2}-\frac{1}{R_c^2}\right), \tag{3.17}$$

Eq. (3.16) can be written as follows:

$$F_{i\alpha}(R_c)=\sum_{\substack{j\neq i\\(r_{ij}<R_c)}}f_{ij\alpha}, \tag{3.18}$$

where

$$f_{ij\alpha}=q_iq_j\left(\frac{1}{r_{ij}^2}\frac{r_{ij\alpha}}{r_{ij}}-\frac{1}{R_c^2}\frac{r_{ij\alpha}}{R_c}\bigg|_{r_{ij}=R_c}\right) \tag{3.19}$$

is the pair force on ion i due to its interaction with ion j, and $r_{ij\alpha}=r_{j\alpha}-r_{i\alpha}$.

For a pair potential, the virial stress tensor is given by[26]

$$\sigma_{\alpha\beta}(R_c)=\frac{1}{6V}\sum_{i=1}^{N}\sum_{\substack{j\neq i\\(r_{ij}<R_c)}} r_{ij\alpha}f_{ij\beta}, \tag{3.20}$$

where $V=N\Omega$ is the system volume and Ω is the average volume per ion. Combining Eqs. (3.19) and (3.20), we thus obtain

$$\sigma_{\alpha\beta}(R_c)=\frac{1}{6V}\sum_{i=1}^{N}\sum_{\substack{j\neq i\\(r_{ij}<R_c)}} q_iq_j \times\left(\frac{1}{r_{ij}^2}\frac{r_{ij\alpha}r_{ij\beta}}{r_{ij}}-\frac{1}{R_c^2}\frac{r_{ij\alpha}r_{ij\beta}}{R_c}\bigg|_{r_{ij}=R_c}\right). \tag{3.21}$$

The manner in which the truncation term in both the forces [Eq. (3.19)] and stresses [Eq. (3.21)] is actually evaluated at R_c is illustrated in Fig. 11. For example, in the case of the stresses, for each $i-j$ pair the angular term associated with the truncation term, $(r_{ij\alpha}r_{ij\beta}/R_c^2)_{r_{ij}=R_c}$, is identical to the angular term, $r_{ij\alpha}r_{ij\beta}/r_{ij}^2$, associated with the corresponding unshifted $i-j$ interaction. This can be interpreted as having added an image charge, $-q_j$, at R_c which compensates the charge q_j at r_{ij} such that ion i effectively interacts only with neutral pairs. The image-charge potential, $-q_iq_j/R_c$, is then added to the unshifted Coulomb potential, q_iq_j/r_{ij}, so as to achieve charge neutralization in the energy and all its derivatives.

For a *cubic* crystal at zero temperature, Eq. (3.21) can be simplified since, for every crystal shell with radius r_s containing $n(r_s)$ ions, one can write

$$\sum_{j=1}^{n(r_s)} r_{ij\alpha}r_{ij\beta}=\delta_{\alpha\beta}\frac{1}{3}r_s^2, \tag{3.22}$$

where $\delta_{\alpha\beta}$ is the Kronecker delta. Inserting Eqs. (3.22) and (3.14) into Eq. (3.21) and substituting for $V_{\rm sh}^C$, after minor manipulation we obtain

$$\sigma_{\alpha\beta}(R_c)=\frac{\delta_{\alpha\beta}}{6\Omega}\frac{1}{3}\sum_{\substack{j\neq i\\(r_{ij}<R_c)}} V_{\rm sh}^C(r_{ij})=\frac{\delta_{\alpha\beta}}{6\Omega}\frac{1}{3}E_i^{\rm Mad}(R_c). \tag{3.23}$$

Consequently, in units of $(6\Omega)^{-1}$, the pressure is identical to one third of the Madelung energy of the perfect-crystal ions, with an identical convergence behavior.

It is interesting to note that the first derivative of $V_{\rm sh}^C(r_{ij})$ in Eq. (3.17), and hence the associated forces and stresses in Eqs. (3.19) and (3.21), are smoothly shifted to zero at the cutoff radius, as is the pair potential in Eq. (3.19) itself. Naturally, all higher derivatives will therefore be truncated in the same manner. An interesting feature of this type of truncation (by an r_{ij}-independent, constant shift) is that it does not alter the shape of the original, unshifted pair potential nor the functional forms of its derivatives. Specifically in the Coulomb case, this implies that the $r^{-(n+1)}$ functional form of the nth derivative of the original Coulomb pair potential is unaffected by the truncation.

D. Discussion

Based on the concept of charge neutralization, Eq. (3.11) describes a pair potential that smoothly approaches zero at the surface of the spherically truncated volume because the charge within this sphere is compensated by an equal and opposite surface charge at R_c (Fig. 11). Interestingly, this is very similar to the classic problem of determining the potential at the center of a conducting, grounded sphere due to the presence of a point charge, q, at some point $\mathbf{r}=r\hat{\mathbf{n}}$ within the sphere (i.e., $r<R_c$); here $\hat{\mathbf{n}}$ is the radial unit vector.[17] Since the sphere is conducting and grounded, the electrostatic potential on its surface must be zero, i.e., $\Phi(R_c)=0$. This condition can be guaranteed by placing a fictitious image charge, $q'=-qR_c/r$, outside the sphere at $\mathbf{r}'=(R_c^2/r)\hat{\mathbf{n}}$. A little analysis[17] then shows that the net induced charge on the conducting sphere is precisely $-q$, i.e., it exactly compensates for the charge inside the sphere, and it is distributed on the conducting shell in a region centered around the point at $R_c\hat{\mathbf{n}}$. The potential at the origin is then simply the sum of the contributions due to the real charge and its image. If there are a number of charges within the spherical shell, the potential at the origin can be simply calculated by linear superposition over the contributions from the charges and their respective images. Thus, in analogy with the charge-neutralization method, the conducting shell also neutralizes the charges that lie within it.

This image-charge method is related to Friedman's reaction-field method[27] in which the charges within a spherical shell of radius R_c are embedded in a dielectric medium of dielectric constant, ϵ. In the reaction-field method the image of the charge q at $\mathbf{r}=r\hat{\mathbf{n}}$ is placed *outside* the truncation sphere at $\mathbf{r}'=(R_c^2/r)\hat{\mathbf{n}}$ and assigned a charge $q'=-(\epsilon-1)/(\epsilon+1)qR_c/r$. In spite of these similarities, the two methods differ qualitatively in three key aspects. First, the physics of the reaction-field and the charge-neutralization methods are different. In the reaction-field method, the image charges describe the response of the embedding dielectric medium (i.e., beyond R_c); in the charge-neutralization method the charges placed on the surface compensate the excess charge within R_c. Second, for $\epsilon\to\infty$ the explicit r dependence in q' leads to a functional form for the force different from that in Eq. (3.19), although it also goes to zero at R_c. Third, for finite ϵ the force on an ion at R_c together with that on its image is finite, whereas beyond R_c the potential, and hence the force, is by definition zero; for finite ϵ the reaction-field method does therefore not provide a suitable basis for a dynamical computational scheme.

The properties of the Coulomb pair potential in Eq. (3.13) suggest a general truncation procedure applicable to all types of pair potentials. That is, by defining a shifted potential, $V_{\rm sh}(r_{ij})$, in terms of the unshifted potential, $V(r_{ij})$, by

$$V_{\rm sh}(r_{ij})=V(r_{ij})-\lim_{r_{ij}\to R_c}\{V(r_{ij})\}, \tag{3.24}$$

one assures not only that at R_c *all* derivatives of $V_{\rm sh}(r_{ij})$ approach zero smoothly but also that the functional form of the unshifted potential and all its derivatives are preserved. In that sense, the truncation method based on Eq. (3.24) is as unintrusive as one might imagine.

In molecular-dynamics simulations, a system whose forces are derived from Eq. (3.24) should, at least in principle, not conserve energy because the energy does not represent quite the correct integral of the forces; when integrating, for example, a ''shifted-force'' potential,[26] a term proportional to r_{ij} appears in the energy. Although the energy and its derivatives are therefore not entirely consistent with one another, our shifting method has the advantage that the actual values for the energy, forces, etc. thus obtained are as close as desirable to the correct ones, i.e., to those obtained for the unshifted pair potential (the exact solution). As illustrated in Sec. VII, however, in practice energy is conserved rather well, permitting the use of the same integration time step as in the full Ewald method.

IV. CONVERGENCE ANALYSIS

According to Fig. 5, the R_c dependent Madelung energy extracted from the spherically truncated, charge-neutralized environments of the ions [see Fig. 2(c)] differs systematically from that obtained from the molecular approach[11] [see Fig. 2(a)]. The likely cause for these differences is that spherical truncation breaks up the molecules near R_c, thus destroying the r^{-5} interaction of an ion with a neutral, molecular shell [see Eq. (2.4)]. As also noted above, the oscillations in the Madelung energy extracted from spherical truncation are of a different nature than the more or less random, much shorter-period fluctuations in the charge density of the system (see, e.g., Figs. 5 and 6). Also, as clearly seen in Fig. 8, the oscillations in the Madelung energy about its fully converged value are weakly damped, with an amplitude roughly decreasing proportional to $1/R_c$. In the following we will elucidate the origin of this behavior by using an analysis based on the charge distribution function, $Q(r)$.

A. Formal analysis

In ionic systems two structural measures are equally useful, the radial distribution function, $G(r)$, and the radial charge distribution function, $Q(r)$. For simplicity, here we limit ourselves to a binary system, with charges $q_i=\pm q$. It is well known that for such a system

$$G(r)=G_{++}(r)+G_{--}(r)+2G_{+-}(r), \tag{4.1}$$

$$Q(r)=G_{++}(r)+G_{--}(r)-2G_{+-}(r), \tag{4.2}$$

where the $G_{\alpha\beta}(r)$ $(\alpha,\beta=+,-)$ are partial radial distribution functions for the different combinations of the two species. Throughout, we use the normalization that for $r\to\infty$, $G(r)$ approaches the average number density of the system; the dimensions of both $G(r)$ and $Q(r)$ are therefore 1/volume. With this definition of $Q(r)$, the average charge between distances r and $r+dr$ from the center of some ion i is given by $q_i 4\pi r^2 Q(r)dr$.

We first consider the convergence behavior of the *charged* system [see, e.g., Fig. 2(c)]. With the above definition of $Q(r)$, the average Coulomb energy per ion may be written as follows [see also Eq. (3.4)]:

$$E^{\mathrm{tot}}(R_c)/N=4\pi q^2\int_0^{R_c} dr\, rQ(r). \tag{4.3}$$

The radial charge distribution function can be represented by its Fourier transform as[28]

$$Q(r)=\frac{1}{2\pi^2 r}\int_0^\infty dk\, k[Q(k)-1]\sin(rk), \tag{4.4}$$

with the spherically averaged charge structure factor given by

$$Q(k)=1+\frac{4\pi}{k}\int_0^\infty dr\, rQ(r)\sin(rk). \tag{4.5}$$

Combining Eqs. (4.3) and (4.4), we obtain

$$E^{\mathrm{tot}}(R_c)/N=\frac{2}{\pi}q^2\int_0^{R_c}dr\int_0^\infty dk\, k[Q(k)-1]\sin(rk); \tag{4.6}$$

integration over r yields

$$E^{\mathrm{tot}}(R_c)/N=\frac{2}{\pi}q^2\int_0^\infty dk[Q(k)-1] -\frac{2}{\pi}q^2\int_0^\infty dk[Q(k)-1]\cos(kR_c). \tag{4.7}$$

This expression reveals that the energy of the charged system consist of two terms, an R_c independent term governed solely by the charge distribution in the system and an R_c dependent term. The actual R_c variation of the second term can only be established assuming a specific form of $Q(k)$. For example, for a completely uncorrelated system, $Q(k)\equiv 1$, i.e., the second term vanishes. On the other hand, for a perfect crystal lattice $Q(k)$ consists of a descrete set of delta functions [see Eq. (4.22) below]; the second term is then simply a sum of nonconvergent oscillatory terms, a finding that is consistent with our numerical results for the perfect NaCl crystal shown in the doubly logarithmic plot in Fig. 12 (open symbols).

The fact that in a perfect crystal lattice the oscillations do not die out means that $E^{\mathrm{tot}}(R_c)/N$ does not converge. Indeed, in a little known paper Emersleben[29] proved half a century ago that in three dimensions the spherically truncated NaCl lattice sum does not converge. However, Borwein *et al.*[30] showed more recently that, by contrast, in a two-dimensional (2D) square lattice spherical truncation converges and that the lack of convergence in the 3D NaCl lattice is intimately connected with the nature of the spherical truncation; they also showed that *cubic* truncation converges in both two and three dimensions.[30] This greater robustness of cubic truncation in the NaCl lattice is probably due to the fact that the crystallographic unit cell and, hence, any system thus generated, is always charge neutral.

Next we consider the convergence behavior of the *charge-neutralized* system. To determine the average Madelung energy per ion[16] [see Eq. (3.6)],

$$E^{\mathrm{Mad}}_{\mathrm{tot}}(R_c)/N=E^{\mathrm{tot}}(R_c)/N-\frac{1}{N}\sum_{i=1}^{N}\frac{q_i\Delta q_i(R_c)}{R_c}, \tag{4.8}$$

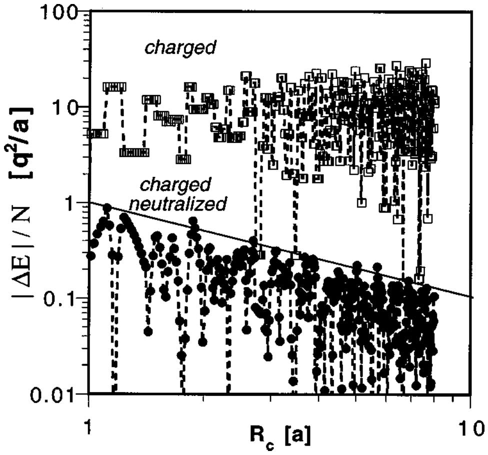

FIG. 12. Comparison of the spherically truncated, charged and charge-neutralized Coulomb energies for the NaCl structure at zero temperature (see also Fig. 4). Open symbols: Log–log plot of the absolute value, $|E^{\mathrm{tot}}(R_c)-E^{\mathrm{Mad}}_{\mathrm{tot}}(R_c\to\infty)|/N$, of the difference between the total energy of the *charged* system and the fully converged Madelung energy, $E^{\mathrm{Mad}}_{\mathrm{tot}}(\infty) = -3.495\,116q^2/a$ [see Eq. (4.13)]. Closed symbols: Same plot for the *charge-neutralized* energy, $|E^{\mathrm{Mad}}_{\mathrm{tot}}(R_c)-E^{\mathrm{Mad}}_{\mathrm{tot}}(R_c\to\infty)|/N$ [see Eq. (4.14)]. The solid line, with a slope of -1, represents $1/R_c$.

we need to calculate the average charge within the cutoff sphere. With the above definition of $Q(r)$, this charge is given by

$$\Delta q_i(R_c)=q_i+4\pi q_i\int_0^{R_c}dr r^2 Q(r), \tag{4.9}$$

where q_i accounts for the central charge not included in $Q(r)$. Inserting the Fourier representation of $Q(r)$ given by Eq. (4.4), integrating by parts over r, dividing by R_c, and using the fact that the integral of $\sin(x)/x$ from zero to infinity is equal to $\pi/2$, we obtain

$$\Delta q_i(R_c)=-\frac{2R_c q_i}{\pi}\int_0^\infty dk[Q(k)-1]\cos(kR_c) + \frac{2q_i}{\pi}\int_0^\infty dk Q(k)\frac{\sin(kR_c)}{k}. \tag{4.10}$$

According to this result, in a perfect crystal lattice [with $Q(k)$ given by Eq. (4.22)] the R_c dependence of $\Delta q_i(R_c)$ is dominated by the first term, revealing that the amplitude of the oscillations in $\Delta q_i(R_c)$ *increases* linearly with R_c. The charge-neutralizing energy, $\Delta q_i(R_c)/R_c$, then becomes equal and opposite to the undamped, oscillatory term in the energy of the spherically truncated, *charged* NaCl lattice [see also Eq. (4.7)]. For a perfect crystal lattice the charge neutralization in Eq. (4.8) therefore completely eliminates the undamped oscillations. This damping effect is clearly visible in Fig. 12 (closed symbols), showing that the solid line with a slope of -1 [see Eq. (4.23) below] represents an envelope for the damped oscillations in $|E^{\mathrm{Mad}}(R_c)-E^{\mathrm{Mad}}(\infty)|$.

Finally, insertion of Eqs. (4.10) and (4.7) into Eq. (4.8) yields the following general expression for the energy of the charge-neutralized system:

$$E^{\mathrm{Mad}}_{\mathrm{tot}}(R_c)/N=\frac{2}{\pi}q^2\int_0^\infty dk[Q(k)-1] - \frac{2}{\pi R_c}q^2\int_0^\infty dk Q(k)\frac{\sin(kR_c)}{k}. \tag{4.11}$$

Similar to Eq. (4.7), the energy of the charge-neutralized system therefore consist of two terms as well, an R_c independent term [identical to the first term in Eq. (4.7)] and a second term, however with a modified R_c dependence. Due to the $1/R_c$ prefactor, this term is responsible for the convergence of the energy of the charge-neutralized system. In fact, even without any charge ordering [i.e., $Q(k)\equiv 1$], this term converges monotonically as $1/R_c$. Incorporation of charge ordering can be expected to speed this convergence significantly since the charges tend to screen their potential and leave the net charge within the truncation sphere as neutral as possible, a fact borne out by all our simulations of the crystal and the melt (see Fig. 8).

The R_c-independent constant in Eqs. (4.7) and (4.11) is readily seen to be identical to the fully converged Madelung energy per ion, $E^{\mathrm{Mad}}_{\mathrm{tot}}(R_c\to\infty)/N$. Inserting Eq. (4.5) for $Q(k)$ and evaluating the integral over k, the constant term becomes

$$E^{\mathrm{Mad}}_{\mathrm{tot}}(R_c\to\infty)/N=\frac{2}{\pi}q^2\int_0^\infty dk[Q(k)-1] = 4\pi q^2\int_0^\infty dr r Q(r). \tag{4.12}$$

Comparison with Eq. (4.3) reveals that this term is identical to $E^{\mathrm{tot}}(R_c\to\infty)/N$ which, by definition, represents the average Madelung energy per ion, $E^{\mathrm{Mad}}_{\mathrm{tot}}(R_c\to\infty)/N$, given by the conditionally convergent infinite sum in Eq. (1.1). That the energies of both the charged and the charge-neutralized systems oscillate about the same Madelung energy is consistent with all the simulation results presented in Sec. III (see Figs. 4, 5, and 7–10). Our principal results, Eqs. (4.7) and (4.11), may therefore be summarized as follows:

$$E^{\mathrm{tot}}(R_c)/N=E^{\mathrm{Mad}}_{\mathrm{tot}}(R_c\to\infty)/N-\frac{2q^2}{\pi}\int_0^\infty dk[Q(k)-1] \times\cos(kR_c), \tag{4.13}$$

$$E^{\mathrm{Mad}}_{\mathrm{tot}}(R_c)/N=E^{\mathrm{Mad}}_{\mathrm{tot}}(R_c\to\infty)/N - \frac{2q^2}{\pi R_c}\int_0^\infty dk Q(k)\frac{\sin(kR_c)}{k}. \tag{4.14}$$

In summary, by contrast with the nonconvergent energy of the charged system in Eq. (4.13), the Madelung energy of the charge-neutralized system in Eq. (4.14) converges at least as $1/R_c$. The factor of $1/k$ under the integral in Eq. (4.14) has the effect of reducing the contributions from the large k vectors such that the lowest k vectors for which $Q(k)$ has a significant value dominate.

B. Discussion

It is interesting to compare the convergence behavior of the spherically truncated, charge-neutralized system in Eq. (4.14) with the R_c^{-2} convergence of the molecular system considered in Sec. II B. According to Eq. (2.5), this requires determination of the interaction energy of each ion with all the ions outside the cutoff sphere. Using the condition of charge neutrality, it can be shown that this energy is equal and opposite to the damped, oscillatory term in Eq. (4.14), i.e., Eq. (2.5) yields $\Delta E^{\mathrm{Mad}}(R_c) \sim 1/R_c$. The charge-neutralized potential in Eq. (4.14) therefore converges less fast than that for the molecular system, a difference arising from the different manners in which the central ion in Figs. 2(a) and 2(c) is surrounded. This comparison demonstrates how the approximate nature of Eq. (3.2), placing the charge-neutralizing ions on the truncation sphere rather than at their correct crystallographic positions, affects the convergence.

For a numerical comparison of Eqs. (4.13) and (4.14) with our simulation results, $Q(k)$ has to be determined explicitly for any given structure. In principle, $Q(k)$ can be obtained from Eq. (4.5), i.e., by integrating over $Q(r)$ associated with the system. Unfortunately, for crystalline systems this approach is not straightforward because for $r \to \infty$, $Q(r)$ does not approach zero due to the presence of long-range order. Instead, we use the relationship[28]

$$Q(k) = \langle Q(\mathbf{k}) \rangle_{|\mathbf{k}|} = \int_{|\mathbf{k}|=k} d\mathbf{s} Q(\mathbf{k})/4\pi k^2, \tag{4.15}$$

where the angular brackets indicate an angular average over a sphere, $\mathbf{s}$, at constant $|\mathbf{k}| = k$. As a consequence of this definition, for any function $f(k)$,

$$4\pi \int dk k^2 f(k) Q(k) = \int d^3\mathbf{k} f(k) Q(\mathbf{k}). \tag{4.16}$$

The charge structure factor, $Q(\mathbf{k})$, in Eq. (4.15) is defined as the square of the Fourier transform of the charge density, $\sigma(\mathbf{r})$, i.e., $Q(\mathbf{k}) = \sigma(\mathbf{k})\sigma^*(\mathbf{k})$. By definition, $\sigma(\mathbf{k})$ is given by

$$\begin{aligned}\sigma(\mathbf{k}) &= \frac{1}{qN^{1/2}} \int d^3\mathbf{r}\, \sigma(\mathbf{r}) \exp[i(\mathbf{k}\cdot\mathbf{r})] \\ &= \frac{1}{qN^{1/2}} \sum_{j=1}^{N} q_j \exp[i(\mathbf{k}\cdot\mathbf{r}_j)],\end{aligned} \tag{4.17}$$

where $\sigma(\mathbf{r}) = \Sigma_j q_j \delta(\mathbf{r}-\mathbf{r}_j)$ is the charge density [to be distinguished from the atomic density, $\rho(\mathbf{r}) = \Sigma_j \delta(\mathbf{r}-\mathbf{r}_j)$]. The normalization factor, $1/qN^{-1/2}$, was introduced here in order for $Q(\mathbf{k})$ to be consistent with the definition of $Q(k)$ given by Eq. (4.5). The charge structure factor $Q(\mathbf{k})$ then becomes [noting that, since $\sigma(\mathbf{r})$ is real, $\sigma^*(\mathbf{k}) = \sigma(-\mathbf{k})$]

$$\begin{aligned}Q(\mathbf{k}) &= \sigma(\mathbf{k})\sigma^*(\mathbf{k}) \\ &= \sigma(\mathbf{k})\sigma(-\mathbf{k}) \\ &= \frac{1}{Nq^2} \int\int d^3\mathbf{r}\, d^3\mathbf{r}'\, \sigma(\mathbf{r})\sigma(\mathbf{r}') \exp[i\mathbf{k}\cdot(\mathbf{r}-\mathbf{r}')],\end{aligned} \tag{4.18}$$

i.e., $Q(\mathbf{k})$ is the Fourier transform of the two-point, charge–charge correlation function, $\sigma(\mathbf{r})\sigma(\mathbf{r}')$, normalized by the number of ions and q^2; its spherical average is therefore the Fourier transform of the spherical average of $\sigma(\mathbf{r})\sigma(\mathbf{r}')$, i.e., $\langle \sigma(\mathbf{r})\sigma(\mathbf{r}') \rangle_{|\mathbf{r}-\mathbf{r}'|} = \langle Q(\mathbf{r}-\mathbf{r}') \rangle_{|\mathbf{r}-\mathbf{r}'|} = Q(r-r')$ [see Eq. (4.5)].

For a perfect crystal lattice, $Q(\mathbf{k})$ defined in Eq. (4.18) vanishes for all $\mathbf{k}$ vectors except those representing reciprocal-space vectors associated with *charged* lattice planes (*hkl*), for which there is constructive interference; therefore $|\sigma(\mathbf{k}_{hkl})| = N^{1/2}$ and hence $Q(\mathbf{k}_{hkl}) = N$. For example, in the rocksalt structure, the charged lattice planes are those for which all three Miller indices are odd. The first peak in $Q(\mathbf{k})$ therefore appears at $|\mathbf{k}_{111}| = 2\pi/d(111)$ corresponding to the most widely spaced *charged* planes in this structure. For a finite-sized, periodically repeated NaCl crystal we may therefore write

$$Q(\mathbf{k}) = N \sum_{(hkl)}^{\mathrm{odd}} \delta_{\mathbf{k}-\mathbf{k}_{hkl}}, \tag{4.19}$$

where $\delta_{\mathbf{k}-\mathbf{k}_{hkl}}$ is the Kronecker delta. For an infinite system $(N \to \infty)$, the Kronecker function is replaced by the properly normalized three-dimensional Dirac delta function,

$$Q(\mathbf{k}) = \rho(2\pi)^3 \sum_{(hkl)}^{\mathrm{odd}} \delta(\mathbf{k}-\mathbf{k}_{hkl}), \tag{4.20}$$

where ρ is the atomic density. Inserting Eq. (4.20) into Eq. (4.15), we finally obtain the desired angular average of $Q(\mathbf{k})$:

$$\begin{aligned}Q(k) &= \rho(2\pi)^3 \sum_{(hkl)}^{\mathrm{odd}} \langle \delta(\mathbf{k}-\mathbf{k}_{hkl}) \rangle_{|\mathbf{k}|} \\ &= \rho(2\pi)^3 \sum_{(hkl)}^{\mathrm{odd}} \frac{\delta(k-|\mathbf{k}_{hkl}|)}{4\pi k^2}.\end{aligned} \tag{4.21}$$

By introducing multiplicity factors, M_{hkl}, which simply count the number of distinct crystallographic directions belonging to a given $\{hkl\}$ family, and substituting $\rho = 8/a^3$ for the NaCl lattice, $Q(k)$ can be finally written as

$$Q(k) = \frac{16\pi^2}{a^3} \sum_{\{hkl\}}^{\mathrm{odd}} M_{hkl} \frac{\delta(k-|\mathbf{k}_{hkl}|)}{k^2}. \tag{4.22}$$

This expression enables us to explicitly determine the oscillatory Madelung energy for the perfect NaCl crystal as a function of R_c. Inserting Eq. (4.22) into Eq. (4.14), we obtain

$$\begin{aligned}E_{\mathrm{tot}}^{\mathrm{Mad}}(R_c)/N &= E_{\mathrm{tot}}^{\mathrm{Mad}}(R_c \to \infty)/N - \frac{32\pi q^2}{R_c a^3} \\ &\quad \times \sum_{\{hkl\}}^{\mathrm{odd}} \frac{M_{hkl}}{|\mathbf{k}_{hkl}|^3} \sin(|\mathbf{k}_{hkl}| R_c).\end{aligned} \tag{4.23}$$

Because of the $|\mathbf{k}_{hkl}|^{-3}$ term, the leading contribution to the $\{hkl\}$ sum arises from the $\{111\}$ planes that represent the most widely spaced charged planes in the rocksalt structure. With $M_{111} = 8$, and $|\mathbf{k}_{111}| = 2\pi/d(111) = 2\pi\sqrt{3}/a$, Eq. (4.23) yields

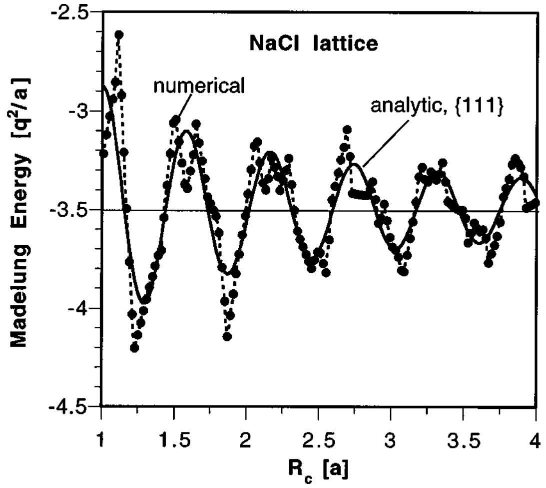

FIG. 13. Comparison of the Madelung energies, $E_{111}^{\mathrm{Mad}}(R_c)/N$, for the NaCl lattice obtained analytically from the approximate expression (4.24) with those determined directly via spherically truncated $1/r$ summation with charge neutralization [see Fig. 5 and Eq. (3.3)].

$$E_{\mathrm{tot}}^{\mathrm{Mad}}(R_c)/N \approx E_{111}^{\mathrm{Mad}}(R_c)/N = E_{\mathrm{tot}}^{\mathrm{Mad}}(R_c \to \infty)/N - \frac{32\sqrt{3}q^2}{9\pi^2 R_c}\sin(2\pi\sqrt{3}R_c/a). \tag{4.24}$$

Figure 13 illustrates that the oscillations in the Madelung energies obtained via spherical truncation of the NaCl lattice with charge neutralization [see Fig. 5 and Eq. (3.3)] are, indeed, reasonably well approximated by the (111) contribution alone given by Eq. (4.24). The differences between $E_{111}^{\mathrm{Mad}}(R_c)/N$ and the numerical data in Fig. 13 arise from the higher-$|\mathbf{k}_{hkl}|$ contributions. We have verified that inclusion in Eq. (4.23) of the five densest charged planes in the NaCl lattice [(111), (311), (331), (333) and (511)] represents the numerical data much better.

In the high-temperature perfect crystal the contribution from the lowest k value, $|\mathbf{k}_{111}|$, in Eq. (4.23) can be expected to dominate even more than in the zero-temperature structure because the peaks in $Q(k)$ are damped by the Debye–Waller factor, $Q(k)=Q(k,T=0)\exp(-k^2\langle u^2\rangle/3)$, where $\langle u^2\rangle$ is the average vibrational amplitude of the ions about their perfect-crystal equilibrium lattice sites.[28] As a consequence, the oscillations in the high-temperature data are much smoother and of smaller amplitude than the zero-temperature results (see Fig. 8), although the $1/R_c$ damping is the same in the two cases.

By contrast with either the zero or the high-temperature crystal, for the melt the oscillations not only in the Madelung energy in Eq. (4.14) but even in the energy of the charged system given by Eq. (4.13) decay with increasing R_c [see also Fig. 7(b)]. This behavior originates from the fact that, because the melt lacks long-range order, its $Q(k)$ does not exhibit the crystalline delta-function peaks. Instead, the key feature in $Q(k)$ is a broad maximum at a $k \sim |\mathbf{k}_{111}|$ associated with the short-range order in the melt; also, for larger k values, $Q(k) \to 1$.[31] The Fourier transform of $Q(k)-1$ in Eq. (4.13) is therefore localized in real space, i.e., it decays with increasing R_c. For the melt the effect of charge neutralization [which gives rise to the $1/R_c$ prefactor in Eq. (4.14)] is therefore merely to speed up the convergence in the Madelung energy.

Based on Eq. (4.14) we can also, at least qualitatively, understand the lack of convergence of the surface and GB energies in Figs. 10(a) and 10(b). We start with the definition of the interface energy, γ, as the Gibbsian excess energy per unit area, A,

$$\gamma = \frac{1}{A}\sum_{n=1}^{n_{\max}} [E_n^{\mathrm{Mad}}(R_c) - E_{\mathrm{pc}}^{\mathrm{Mad}}(R_c)], \tag{4.25}$$

where $E_n^{\mathrm{Mad}}(R_c)$ is the charge-neutralized energy of all the N_p ions located in a given plane n near the (hkl) interface plane while $E_{\mathrm{pc}}^{\mathrm{Mad}}(R_c)$ is the corresponding perfect-crystal reference energy. The sum includes all lattice planes within the distance R_c from the interface, i.e., $n_{\max}=R_c/d(hkl)$, where $d(hkl)$ is the interplanar spacing.

According to Eq. (4.14), $E_n^{\mathrm{Mad}}(R_c)$ is given by

$$E_n^{\mathrm{Mad}}(R_c)/N_p = E_n^{\mathrm{Mad}}(R_c \to \infty)/N_p - \frac{2q^2}{\pi R_c}\int_0^\infty dk Q_n(k)\frac{\sin(kR_c)}{k}, \tag{4.26}$$

where, in analogy to Eq. (4.5), $Q_n(k)$ is defined as the Fourier transform of the radial charge distribution function, $Q_n(r)$, averaged over the N_p ions in plane n. Both $E_n^{\mathrm{Mad}}(R_c)$ and the perfect-crystal energies in Eq. (4.25) therefore converge in the same oscillatory manner, and have an amplitude that decreases as $1/R_c$. However, because the total number of terms in Eq. (4.25), $n_{\max}=R_c/d(hkl)$, *increases* linearly with R_c, the effective damping in γ is greatly reduced. In fact if one were to assume that the energy differences in Eq. (4.25) are entirely independent of n, the oscillations in the resulting expression for γ would become entirely undamped. That this assumption is actually not too unreasonable is seen from our simulation results in Figs. 10(a) and 10(b) that reveal an approximately constant amplitude of the oscillations in γ.

V. EFFECTS OF DAMPING THE PAIR POTENTIAL

In Sec. IV the theoretical foundations were developed based on which the true Madelung potential[16] of the ions can be extracted simply by neutralizing the total energy of a spherically truncated, charged system. Unfortunately, however, due to its rather slow, $1/R_c$ oscillatory decay the potential thus obtained suffers from practical limitations; moreover, in some cases, particularly in the determination of interfacial excess energies, the oscillations are practically undamped, rendering the method virtually useless for practical applications. Clearly, the numerical accuracy of the method needs to be improved to make it computationally more robust.

At this juncture, we have essentially two choices. One option would be to improve the model for deriving the Madelung potential from the *actual* charge distribution within the spherically truncated volume. For example, one might think of compensating not only for the net charge near the surface of the spherically truncated system but also for the higher moments in the charge distribution by subtracting the relevant expressions from the total energy. This approach is qualitatively similar to the fast-multipole methods developed in recent years for the simulation of Coulombic systems.[8–10] However, the main advantage of the above approach, namely, the conceptual and computational simplicity associated with the assumed δ-function distribution of the net charge in the system on the system surface, would be lost. In our view, giving up this simplicity in favor of having to consider the actual excess-charge distribution within the truncation sphere would be a conceptual step backwards because it would refocus the computational problem on the details of how in each case the ions are surrounded for the purpose of extracting their true Madelung energy. We will therefore not pursue this option here.

Our second option, conceptually less ambitious but operationally extremely useful, is to damp the Coulomb *pair* potential in Eq. (3.13) directly so as to more quickly flatten out the oscillations with increasing R_c in the resulting Madelung energy in Eqs. (3.6) and (4.14). Our analysis in Sec. IV has demonstrated that the effect of neutralizing the surface charge in the spherically truncated system is equivalent to *symmetrically damping* the R_c-dependent Madelung energy of each ion. These results offer hope that damping the underlying pair potential in Eq. (3.13) directly may be equally successful in that damping will not only significantly reduce the value of R_c required to achieve satisfactory numerical precision in actual simulations but also render the value of the fully converged Madelung energy essentially unchanged from its undamped value for $R_c \rightarrow \infty$. While preserving the conceptual and practical simplicity of spherical truncation with surface-charge neutralization, the challenge with this approach is to establish the theoretical foundations that permit the systematic errors introduced by damping the pair potential to be assessed for any particular damping function. In the following we demonstrate that the Ewald method provides a theoretical framework for exactly this type of approach.

A. Damped, charge-neutralized Coulomb pair potential

While, in principle, we could choose any damping function,[32] in the following we only consider damping via the complementary error function. Because of its close connection with the Ewald method and the ease by which the necessary mathematical manipulations can be performed, this choice will enable us to establish the mathematical correspondence between spherically truncated r^{-1} summation and the Ewald method and shed some light on its physical interpretation.

In analogy to the trick applied in Eq. (1.2) to derive the Ewald sum for the infinite system, we start by multiplying the total energy of the system in Eq. (1.1) by unity $[\mathrm{erfc}(x)+\mathrm{erf}(x)=1]$, i.e.,

$$E^{\mathrm{tot}}=\frac{1}{2}\sum_{i=1}^{N}\sum_{j\neq i=1}^{\infty}\frac{q_i q_j\,\mathrm{erfc}(\alpha r_{ij})}{r_{ij}}+\frac{1}{2}\sum_{i=1}^{N}\sum_{j\neq i=1}^{\infty}\frac{q_i q_j\,\mathrm{erf}(\alpha r_{ij})}{r_{ij}}, \tag{5.1}$$

where α is a damping parameter determining how fast the complementary error function falls off from one (at $r_{ij}=0$) to zero with increasing r_{ij}. Our goal now is to subdivide the total energy,

$$E^{\mathrm{tot}}=E^{\mathrm{tot}}_{(1)}+E^{\mathrm{tot}}_{(2)}, \tag{5.2}$$

such that $E^{\mathrm{tot}}_{(1)}$ represents the dominant contribution associated with the damped Coulomb pair potential while $E^{\mathrm{tot}}_{(2)}$ is a correction term that can be made arbitrarily small. Unfortunately, the breakdown of E^{tot} in Eq. (5.1) does not satisfy this condition as the second term becomes very large for large values of α.

A remedy to the problem is to simply add and subtract the self term (for $i=j$) associated with the second contribution in Eq. (5.1),

$$\lim_{r_{ij}\to 0}\left\{\frac{1}{2}\sum_{i=1}^{N}\frac{q_i^2\,\mathrm{erf}(\alpha r_{ij})}{r_{ij}}\right\}=\frac{\alpha}{\pi^{1/2}}\sum_{i=1}^{N}q_i^2, \tag{5.3}$$

on the right-hand side of Eq. (5.1), and subsequently to define $E^{\mathrm{tot}}_{(1)}$ and $E^{\mathrm{tot}}_{(2)}$ as follows:

$$E^{\mathrm{tot}}_{(1)}=\frac{1}{2}\sum_{i=1}^{N}\sum_{j\neq i=1}^{\infty}\frac{q_i q_j\,\mathrm{erfc}(\alpha r_{ij})}{r_{ij}}-\frac{\alpha}{\pi^{1/2}}\sum_{i=1}^{N}q_i^2, \tag{5.4}$$

$$E^{\mathrm{tot}}_{(2)}=\frac{1}{2}\sum_{i=1}^{N}\sum_{j=1}^{N}\frac{q_i q_j\,\mathrm{erf}(\alpha r_{ij})}{r_{ij}}. \tag{5.5}$$

In the following we will assert, both numerically and analytically, that for a range of α values $E^{\mathrm{tot}}_{(2)}$ thus defined, indeed, represents a small correction to $E^{\mathrm{tot}}_{(1)}$. Also, in Sec. VI we will demonstrate that $E^{\mathrm{tot}}_{(2)}$ is identical to the reciprocal-space energy in the Ewald sum; the latter can therefore be viewed as the systematic error introduced when replacing the bare Coulomb pair potential by the damped one. Our discussion follows closely the formal development in Secs. III B and III C, the only differences arising from the replacement of the bare potential by the damped pair potential.

In practice, $E^{\mathrm{tot}}_{(1)}$ can only be evaluated for a finite cutoff radius, R_c. Equation (5.4) is therefore written as follows:

$$E^{\mathrm{tot}}_{(1)}(R_c)=\frac{1}{2}\sum_{i=1}^{N}\sum_{\substack{j\neq i\\(r_{ij}<R_c)}}\frac{q_i q_j\,\mathrm{erfc}(\alpha r_{ij})}{r_{ij}}-\frac{\alpha}{\pi^{1/2}}\sum_{i=1}^{N}q_i^2. \tag{5.6}$$

In analogy to Sec. III B, the charge-neutralized (or "true" Madelung) potential then becomes

$$E^{\mathrm{Mad}}_{\mathrm{tot}}(R_c)\approx E^{\mathrm{tot}}_{(1)}(R_c)-E^{\mathrm{neutr}}_{\mathrm{tot}}(R_c), \tag{5.7}$$

where, by analogy with Eq. (3.5), the energy associated with the charge-neutralizing surface charge is given by

$$E^{\mathrm{neutr}}_{\mathrm{tot}}(R_c)\approx\frac{1}{2}\sum_{i=1}^{N}\frac{q_i\Delta q_i(R_c)\,\mathrm{erfc}(\alpha R_c)}{R_c}. \tag{5.8}$$

Following the development in Sec. III C, this expression may formally be replaced by

$$E_{\text{tot}}^{\text{neutr}}(R_c) \approx \lim_{r_{ij}\to R_c} \left\{ \frac{1}{2}\sum_{i=1}^{N} \sum_{\substack{j\neq i \\ (r_{ij}<R_c)}} \frac{q_i q_j \,\text{erfc}(\alpha r_{ij})}{r_{ij}} \right\} + \frac{\text{erfc}(\alpha R_c)}{2R_c}\sum_{i=1}^{N} q_i^2, \tag{5.9}$$

where the additive constant is a self term for each ion [see also Eq. (3.12)]. The Madelung energy in Eq. (5.7) may then be written as follows:

$$E_{\text{tot}}^{\text{Mad}}(R_c) \approx \frac{1}{2}\sum_{i=1}^{N} \sum_{\substack{j\neq i \\ (r_{ij}<R_c)}} V_{\text{sh}}^{\text{EW}}(r_{ij}) - E_{\text{self}}, \tag{5.10}$$

where the shifted Coulomb pair potential from Eq. (3.13) was replaced by the ''shifted (or charge-neutralized) Ewald potential,''

$$V_{\text{sh}}^{\text{EW}}(r_{ij}) = \frac{q_i q_j \,\text{erfc}(\alpha r_{ij})}{r_{ij}} - \lim_{r_{ij}\to R_c} \left\{ \frac{q_i q_j \,\text{erfc}(\alpha r_{ij})}{r_{ij}} \right\}. \tag{5.11}$$

By analogy with the self term in Eqs. (3.10) and (3.15), the additive constant in Eq. (5.10),

$$E_{\text{self}} = \left(\frac{\text{erfc}(\alpha R_c)}{2R_c} + \frac{\alpha}{\pi^{1/2}} \right) \sum_{i=1}^{N} q_i^2, \tag{5.12}$$

is a self term for each ion that is merely added to the total Madelung energy of the system. Inserting these definitions, Eq. (5.10) may be rewritten more explicitly as follows:

$$E_{\text{tot}}^{\text{Mad}}(R_c) \approx \frac{1}{2}\sum_{i=1}^{N} \sum_{\substack{j\neq i \\ (r_{ij}<R_c)}} \left(\frac{q_i q_j \,\text{erfc}(\alpha r_{ij})}{r_{ij}} - \lim_{r_{ij}\to R_c} \left\{ \frac{q_i q_j \,\text{erfc}(\alpha r_{ij})}{r_{ij}} \right\} \right) - \left(\frac{\text{erfc}(\alpha R_c)}{2R_c} + \frac{\alpha}{\pi^{1/2}} \right) \sum_{i=1}^{N} q_i^2. \tag{5.13}$$

The interpretation of these expressions is the same as that for the undamped potential (see Sec. III C), namely, Eqs. (5.10)–(5.13) describe how, for the damped Coulomb pair potential, the Madelung energy can be extracted from the total energy of the spherically truncated, charged system [see also Figs. 2(a) and 2(c)]. As in Sec. III C, these expressions reveal that the physical concept of charge neutralization at the system surface is equivalent to the operational concept of shifting the pair potential. In Sec. V C, the relevant expressions for the forces and stresses associated with Eq. (5.10) will be derived; these will then provide the basis for the molecular-dynamics simulations discussed in Sec. VII.

Figures 14(a) and 14(b) demonstrate the dramatic improvements due to damping [Eq. (5.13)] in the approach of the Madelung energies of the perfect NaCl crystal and the MgO melt towards their correct values indicated by the dashed horizontal lines. For the value of $\alpha = 0.8/a$ chosen for these illustrations, in both cases the Madelung energy approaches its correct, fully converged Ewald value very rapidly (dashed horizontal line) and, for $R_c \geqslant 2a$, is practically converged. The rapid approach to zero of the underlying damping function, erfc(αr), which is responsible for this behavior, is shown in Fig. 14(a) (right axis).

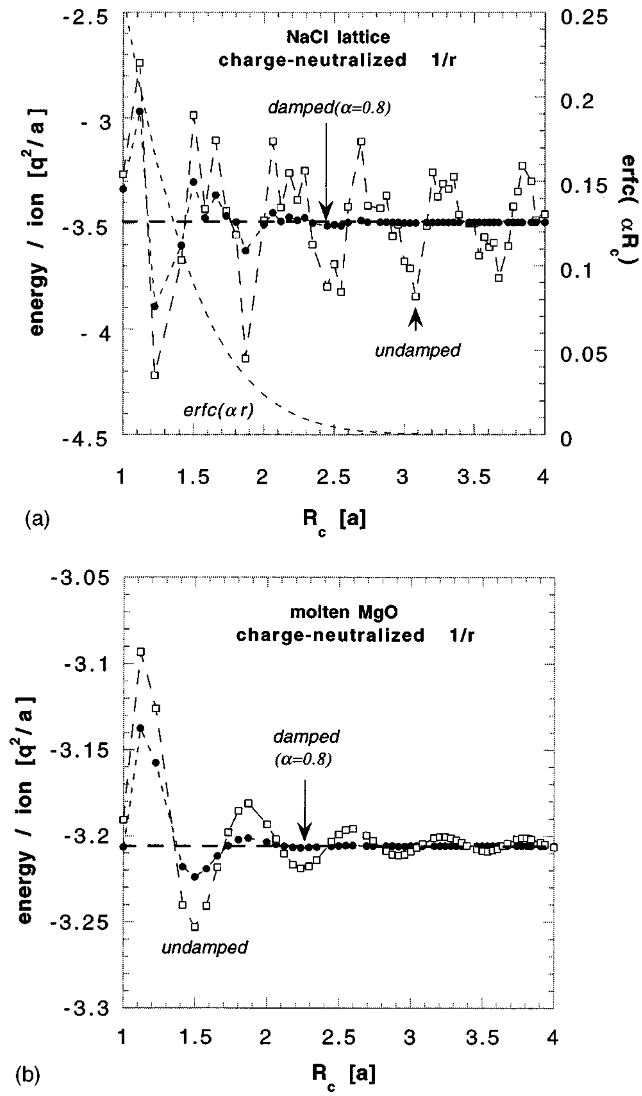

FIG. 14. Comparison of the charge-neutralized damped and undamped Madelung energies for (a) the zero-temperature perfect crystal and (b) the MgO melt for $\alpha = 0.8/a$ [see also Figs. 6 and 7(b)]. In (a) the rapid approach to zero of the underlying damping function, erfc(αR_c) is also illustrated (right axis). The dashed horizontal lines indicate the correct Ewald values.

The particularly dramatic benefits of damping in the case of the interfacial systems are illustrated in Figs. 15(a)–15(c) for the case of the free (100) surface. By contrast with the practically undamped oscillations in the excess energies in Fig. 10(a), the damped energies in Fig. 15(a) converge rapidly to their correct values obtained from Parry's slab version[25] of the Ewald sum (dashed horizontal lines). Remarkably, when increasing the value of α from $0.8/a$ to $1.5/a$, the effective range of the potential decreases from $R_c \approx 2.6a$ to about $1.5a$, with virtually no effect on the value of the fully converged energy.

The equally dramatic effects on the surface stresses (formal expressions for the stresses and forces are given in Sec.

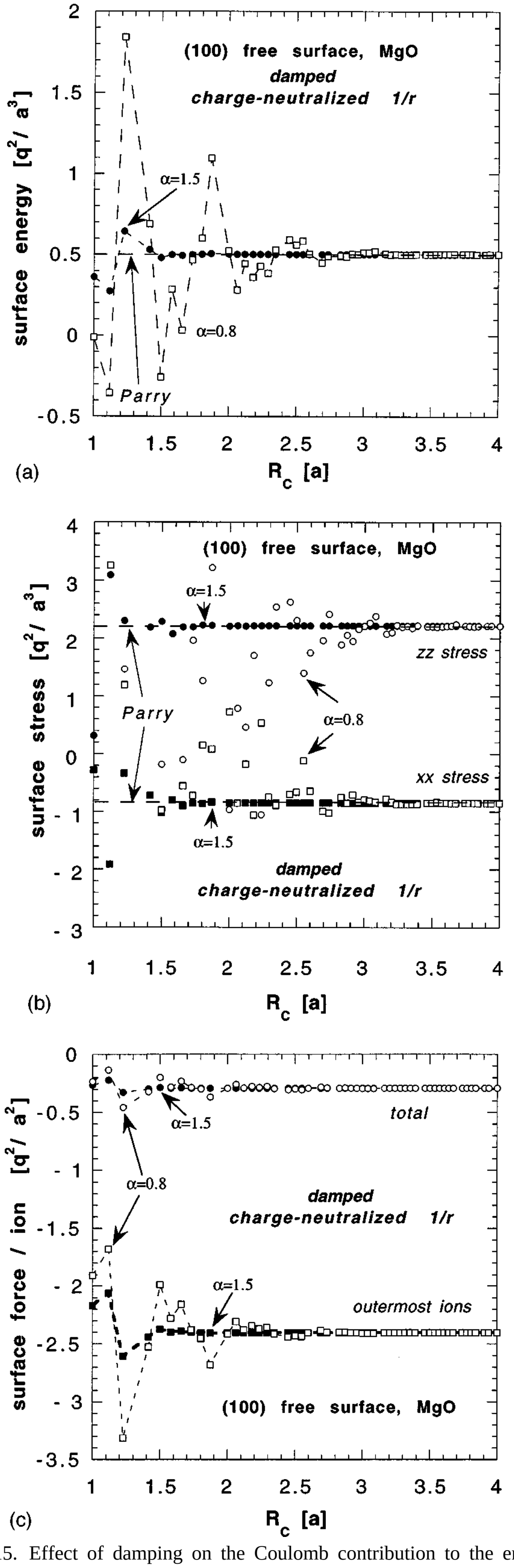

FIG. 15. Effect of damping on the Coulomb contribution to the energy, forces, and stresses of the MgO (100) free-surface at zero temperature. (a) Surface energy for $\alpha=0.8/a$ and $1.5/a$ (in units of q^2/a^3); for comparison, see the undamped surface energy in Fig. 10(a); (b) related surface stresses per unit area parallel (*xx* component) and perpendicular (*zz* component) to the surface (in units of q^2/a^3); (c) force per ion in the outermost plane and total excess force per ion (i.e., integrated over the entire surface region and normalized to the number of ions in the outermost plane; in units of q^2/a^2). The dashed horizontal lines in (a)–(c) indicate the correct Parry values (Ref. 25).

V C) are illustrated in Fig. 15(b), which shows the Gibbsian excess stresses per unit area parallel (*xx* component) and perpendicular (*zz* component) to the surface. We note that the Coulomb stresses shown here are balanced by the stresses associated with the short-range repulsive part of the potential. This is the reason why the *zz* component of the Coulomb stress does not vanish, in spite of the fact that the *total zz* stress vanishes in the fully relaxed surface. By contrast, the *xx* and *yy* components of the total surface stress are usually finite, indicating that the surface would prefer to have a lattice parameter that is different (usually shorter) than that of the bulk crystal.

Finally, shown in Fig. 15(c) are two types of Coulomb forces per ion, the force on each individual ion in the outermost plane and the total excess force per ion (i.e., integrated over the entire surface region and normalized to the number of ions in the outermost plane). Again, since the surface is relaxed, the *total* force on each ion vanishes although the Coulomb forces are finite and balanced by the short-range forces. The remarkable result in Figs. 15(b) and 15(c) is that both the stresses and forces settle down very rapidly to their correct values obtained from the Parry formula,[25] with approximately the same R_c range as the energy in Fig. 15(a).

B. Relationship with real-space Ewald energy

To facilitate the comparison of Eq. (5.13) with the Ewald method, it is useful to rewrite the starting expression for the Ewald sum, Eq. (1.2), in a manner analogous to Eq. (5.4), by simply adding and subtracting on the right-hand side of Eq. (1.2) the self term (for $\mathbf{n=0}$ and $i=j$) associated with the erf(αr) term [see also Eq. (5.3)],

$$\lim_{|\mathbf{n}L|\to 0}\left\{\frac{1}{2}\sum_{i=1}^{N}\frac{q_i^2\,\mathrm{erf}(\alpha|\mathbf{n}L|)}{|\mathbf{n}L|}\right\}=\frac{\alpha}{\pi^{1/2}}\sum_{i=1}^{N}q_i^2. \tag{5.14}$$

The real- and reciprocal-space contributions to the Ewald sum in Eq. (1.5) may then be written as follows:

$$E_{\mathbf{r}}^{\mathrm{tot}}=\frac{1}{2}\sum_{i=1}^{N}\sum_{j=1}^{N}\sum_{\mathbf{n=0}}^{\infty}{}'\,\frac{q_iq_j\,\mathrm{erfc}(\alpha|\mathbf{r}_{ij}+\mathbf{n}L|)}{|\mathbf{r}_{ij}+\mathbf{n}L|}-\frac{\alpha}{\pi^{1/2}}\sum_{i=1}^{N}q_i^2, \tag{5.15}$$

$$E_{\mathbf{k}}^{\mathrm{tot}}=\frac{1}{2}\sum_{i=1}^{N}\sum_{j=1}^{N}\sum_{\mathbf{n=0}}^{\infty}\frac{q_iq_j\,\mathrm{erf}(\alpha|\mathbf{r}_{ij}+\mathbf{n}L|)}{|\mathbf{r}_{ij}+\mathbf{n}L|}, \tag{5.16}$$

where the prime has been omitted in Eq. (5.16), indicating that the self term is now included. By subdividing the Ewald sum in this unconventional manner, similar to the breakdown of the total energy in Eqs. (5.2), (5.4), and (5.5) we assure that in practice $E_{\mathbf{k}}^{\mathrm{tot}}$ represents a small correction to the real-space term, $E_{\mathbf{r}}^{\mathrm{tot}}$. As demonstrated below, this greatly facilitates the comparison between the Ewald sum [Eqs. (1.5), (5.15), and (5.16)] and the damped, direct r^{-1} sum.

An obvious difference between Eq. (5.13) and the real-space Ewald energy in Eq. (5.15) is that the latter implies the system to be periodic. This can sometimes be an advantage because one can then apply the so-called minimum-image

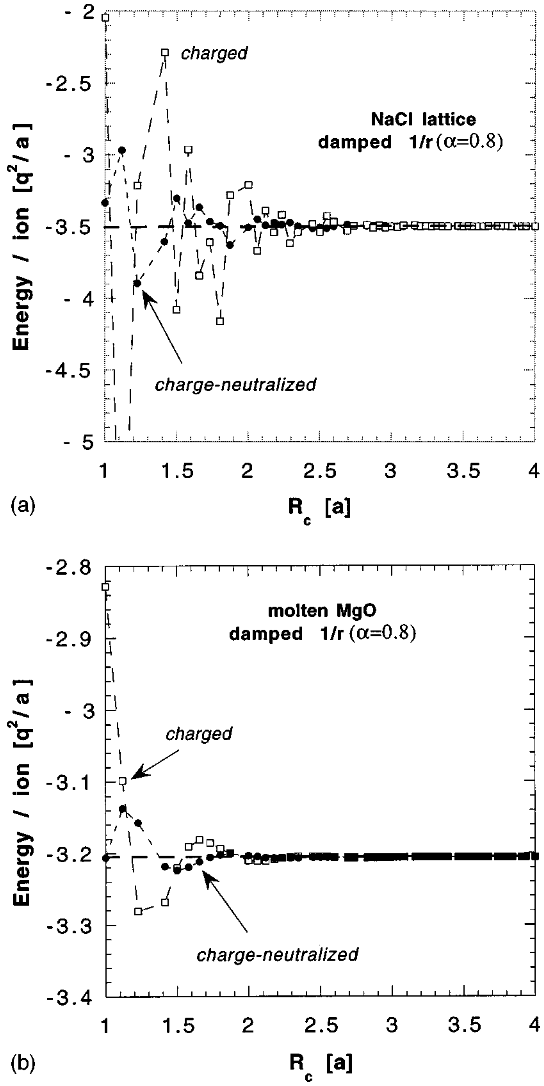

FIG. 16. Effect of charge neutralization (or shifting) on the damped r^{-1} potential for $\alpha=0.8/a$. (a) Zero-temperature perfect crystal; (b) MgO melt. The dashed horizontal lines indicate the Ewald values.

truncation method. By contrast with spherical truncation, in this method every ion is surrounded by the same, full content of the simulation cell. Since the latter is usually neutral, the benefit of minimum-image truncation is that every ion is thus automatically embedded in a neutral environment for the purpose of computing its Coulomb energy. Unfortunately, however, when the simulation cell is rather large or when its shape deviates considerably from a cube, the method is not very practical.

The most important difference between the real-space expressions given by Eqs. (5.13) and (5.15) is that, by contrast with the damped, direct r^{-1} sum in Eq. (5.13), the real-space Ewald expression in Eq. (5.15) is unshifted (i.e., non-neutralized), with a discontinuity of the potential and its derivatives at $r_{ij}=R_c$; Eq. (5.15) therefore represents the $R_c\to\infty$ limit of Eq. (5.13). The effect of shifting on the real-space Ewald potential [i.e., of converting Eq. (5.15) into Eq. (5.13)] is demonstrated in Figs. 16(a) and 16(b) for the perfect crystal and the melt, again for $\alpha=0.8/a$. As expected, in both cases charge neutralization dramatically reduces the magnitude of the oscillations and therefore speeds the convergence towards the correct Madelung energy (dashed horizontal line), the net effect being a reduction in the effective range of the potential.

C. Forces and stresses

Similar to Sec. III C, to facilitate the evaluation of the forces and stresses, our starting equation (5.10) is rewritten as follows [see also Eq. (3.15)]:

$$E_{\text{tot}}^{\text{Mad}}(R_c)\approx\frac{1}{2}\sum_{i=1}^{N} E_i^{\text{Mad}}(R_c)-E_{\text{self}}, \tag{5.17}$$

where, by analogy with Eq. (3.14), the Madelung energy of ion i was defined by

$$E_i^{\text{Mad}}(R_c)=\sum_{\substack{j\neq i\\(r_{ij}<R_c)}} V_{\text{sh}}^{\text{EW}}(r_{ij}). \tag{5.18}$$

We note that

$$\frac{d\,\text{erfc}(\alpha r_{ij})}{dr_{ij}}=-\frac{2\alpha}{\pi^{1/2}}\exp(-\alpha^2 r_{ij}^2); \tag{5.19}$$

the derivative of $V_{\text{sh}}^{\text{EW}}(r_{ij})$ [see Eq. (5.11)] therefore becomes

$$\frac{dV_{\text{sh}}^{\text{EW}}(r_{ij})}{dr_{ij}}=-q_iq_j\left(\frac{\text{erfc}(\alpha r_{ij})}{r_{ij}^2}+\frac{2\alpha}{\pi^{1/2}}\frac{\exp(-\alpha^2 r_{ij}^2)}{r_{ij}}-\frac{\text{erfc}(\alpha R_c)}{R_c^2}-\frac{2\alpha}{\pi^{1/2}}\frac{\exp(-\alpha^2 R_c^2)}{R_c}\right). \tag{5.20}$$

The force on ion i may then be written as follows [see also Eqs. (3.16) and (3.18)]:

$$F_{i\alpha}(R_c)=-\frac{\partial E_i^{\text{Mad}}}{\partial r_{i\alpha}}=-\sum_{\substack{j\neq i\\(r_{ij}<R_c)}}\frac{dV_{\text{sh}}^{\text{EW}}(r_{ij})}{dr_{ij}}\frac{r_{ij\alpha}}{r_{ij}}=\sum_{\substack{j\neq i\\(r_{ij}<R_c)}} f_{ij\alpha}, \tag{5.21}$$

where

$$f_{ij\alpha}=\sum_{\substack{j\neq i\\(r_{ij}<R_c)}} q_iq_j\left\{\left(\frac{\text{erfc}(\alpha r_{ij})}{r_{ij}^2}+\frac{2\alpha}{\pi^{1/2}}\frac{\exp(-\alpha^2 r_{ij}^2)}{r_{ij}}\right)\times\frac{r_{ij\alpha}}{r_{ij}}-\left(\frac{\text{erfc}(\alpha R_c)}{R_c^2}+\frac{2\alpha}{\pi^{1/2}}\frac{\exp(-\alpha^2 R_c^2)}{R_c}\right)\times\frac{r_{ij\alpha}}{R_c}\bigg|_{r_{ij}=R_c}\right\} \tag{5.22}$$

is the pair force on ion i due to its interaction with ion j. Analogous to Eq. (3.21), the virial stress tensor defined in Eq. (3.20) then becomes

$$\sigma_{\alpha\beta}(R_c)=\frac{1}{6V}\sum_{i=1}^{N}\sum_{\substack{j\neq i\\(r_{ij}<R_c)}} q_i q_j\left\{\left(\frac{\mathrm{erfc}(\alpha r_{ij})}{r_{ij}^2}+\frac{2\alpha}{\pi^{1/2}}\right.\right.$$
$$\left.\times\frac{\exp(-\alpha^2 r_{ij}^2)}{r_{ij}}\right)\frac{r_{ij\alpha}r_{ij\beta}}{r_{ij}}-\left(\frac{\mathrm{erfc}(\alpha R_c)}{R_c^2}+\frac{2\alpha}{\pi^{1/2}}\right.$$
$$\left.\left.\times\frac{\exp(-\alpha^2 R_c^2)}{R_c}\right)\frac{r_{ij\alpha}r_{ij\beta}}{R_c}\bigg|_{r_{ij}=R_c}\right\}. \tag{5.23}$$

Because of the exponentials in this expression, a simple relationship between the energy and pressure for *cubic* crystals similar to Eq. (3.23) does not exist for $\alpha>0$. The convergence behaviors of the pressure and the energy are therefore not quite identical although, in practice, the effective R_c range of the charge-neutralized pressure is found to be the same as that of the energy.

VI. ANALYSIS OF THE ERROR TERM

As already mentioned, a critical problem with the operational approach of damping is the illumination of the magnitude and physical nature of the systematic error introduced when replacing the bare r^{-1} pair potential by a damped one. We recall that the purpose of the particular breakdown of $E^{\mathrm{tot}}=E^{\mathrm{tot}}_{(1)}+E^{\mathrm{tot}}_{(2)}$ in Eqs. (5.2), (5.4), and (5.5) was to capture the largest by far contribution to $E^{\mathrm{Mad}}_{\mathrm{tot}}$ in $E^{\mathrm{tot}}_{(1)}$ while ensuring that the systematic error, $\Delta E^{\mathrm{Mad}}_{\mathrm{tot}}\equiv E^{\mathrm{tot}}_{(2)}$, is small for all practical purposes. Starting from Eq. (5.5), our analysis of $\Delta E^{\mathrm{Mad}}_{\mathrm{tot}}$ will closely follow the Ewald method. Apart from making a formal connection with this method, this will enable us to illuminate the physics underlying the reciprocal-space term in the Ewald sum.

A. Formal relationship

To enable Fourier transformation of the expression for $E^{\mathrm{tot}}_{(2)}$ in Eq. (5.5), periodicity has to be imposed on the system. At this point we need not specify whether this periodicity applies to all three dimensions, as in the conventional Ewald method, or to only two dimensions while allowing for finite thickness in the third dimension.[25] In full analogy to the error-function term in Eq. (1.2), the expression for $E^{\mathrm{tot}}_{(2)}$ is therefore rewritten as follows:

$$\Delta E^{\mathrm{Mad}}_{\mathrm{tot}}\equiv E^{\mathrm{tot}}_{(2)}=\frac{1}{2}\sum_{i=1}^{N}\sum_{j=1}^{N}\sum_{\mathbf{n}=\mathbf{0}}^{\infty}\frac{q_i q_j\,\mathrm{erf}(\alpha|\mathbf{r}_{ij}+\mathbf{n}L|)}{|\mathbf{r}_{ij}+\mathbf{n}L|}. \tag{6.1}$$

As discussed above, the self term [for $i=j$ and $\mathbf{n}=\mathbf{0}$; see Eqs. (5.20) and (5.14)] is included in this expression; this term is needed if one wishes to take the Fourier transform of Eq. (6.1).

We note that Eq. (6.1) is identical to the starting expression (5.16) for the reciprocal-space Ewald term. Following the Ewald method, Eq. (6.1) is therefore Fourier transformed. The reciprocal-space term in the Ewald sum thus obtained may be written in the well-known manner as follows:

$$\Delta E^{\mathrm{Mad}}_{\mathrm{tot}}\equiv E^{\mathrm{tot}}_{(2)}\equiv E^{\mathrm{tot}}_{\mathbf{k}}=E^{(\mathbf{k}=\mathbf{0})}+E^{(\mathbf{k}\neq\mathbf{0})}. \tag{6.2}$$

If we assume 3D periodicity in Eq. (6.1), i.e., $\mathbf{n}=(n_x,n_y,n_z)$, the $\mathbf{k}=\mathbf{0}$ and $\mathbf{k}\neq\mathbf{0}$ terms in Eq. (6.2) may be written as follows:

$$E^{(\mathbf{k}=\mathbf{0})}=\frac{2\pi}{3V}\left(\sum_{i=1}^{N}q_i\mathbf{r}_i\right)^2, \tag{6.3}$$

and

$$E^{(\mathbf{k}\neq\mathbf{0})}=\frac{2\pi Nq^2}{V}\sum_{\mathbf{k}\neq\mathbf{0}}^{\infty}\frac{\exp(-k^2/4\alpha^2)}{k^2}Q(\mathbf{k}), \tag{6.4}$$

where V is the simulation-cell volume and $Q(\mathbf{k})$ is the charge structure factor defined in Eq. (4.18).

For a 2D periodic slab geometry, i.e., $\mathbf{n}=(n_x,n_y)$, these terms become considerably more complex.[25] Most important, by contrast with Eqs. (6.3) and (6.4) the double sum involving i and j can no longer be reduced to the square of a single sum.[25] Also, because of the 2D periodicity within the slab plane, with unit-cell area A, the in-plane component of $\mathbf{r}_{ij}$, $\mathbf{p}_{ij}=\{x_{ij},y_{ij}\}$, has to be distinguished from its out-of-plane component, z_{ij}. Following Parry,[25] the $\mathbf{k}=\mathbf{0}$ and $\mathbf{k}\neq\mathbf{0}$ terms in Eq. (6.2) may then be written as follows:

$$E^{(\mathbf{k}=\mathbf{0})}=-\frac{\pi}{A}\sum_{i=1}^{N}\sum_{j=1}^{N}q_i q_j\times\left\{\frac{\exp(-\alpha^2|\mathbf{z}_{ij}|^2)}{\alpha\pi^{1/2}}+|\mathbf{z}_{ij}|\,\mathrm{erf}(\alpha|z_{ij}|)\right\}, \tag{6.5}$$

and

$$E^{(\mathbf{k}\neq\mathbf{0})}=\frac{\pi}{2A}\sum_{i=1}^{N}\sum_{j=1}^{N}q_i q_j\sum_{\mathbf{k}\neq\mathbf{0}}^{\infty}\frac{\exp[i(\mathbf{k}\cdot\mathbf{p}_{ij})]}{k}\times[F(|k,z_{ij}|)+F(k,-|z_{ij}|)], \tag{6.6}$$

where

$$F(k,\pm|z_{ij}|)=\exp(\pm k|z_{ij}|)\,\mathrm{erfc}\left(\frac{k}{2\alpha}\pm\alpha|z_{ij}|\right). \tag{6.7}$$

Because of the explicit z_{ij} dependence, the double sums in Eqs. (6.5) and (6.6) cannot be reduced to a single sum. Apart from the greater mathematical complexity of these terms by comparison with Eqs. (6.3) and (6.4), the fact that these double sums have to be explicitly evaluated makes molecular-dynamics simulations of interfacial systems using Parry's method[25] prohibitively expensive.

Equations (6.1)–(6.7) provide the theoretical framework needed for assessing the nature and magnitude of the systematic error, $\Delta E^{\mathrm{Mad}}_{\mathrm{tot}}(\alpha)$, introduced when replacing the bare Coulomb potential by the damped one. By definition, in the absence of damping (i.e., for $\alpha=0$) the error term vanishes identically; in practice, however, there seems to be no way to avoid a finite value of α because, without some degree of damping, the energy oscillations in the real-space energy, $E^{\mathrm{tot}}_{(1)}$, fall off too slowly, and hence require a rather long truncation radius. As in the Ewald method, the challenge is therefore to identify the optimum compromise between the practical benefits of damping and the systematic errors thus inevitably introduced.

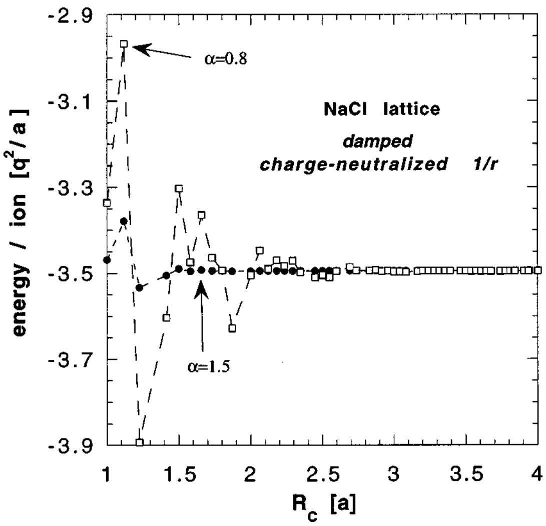

FIG. 17. α dependence of the Madelung energy per ion of the zero-temperature perfect crystal (in units of q^2/a).

B. Simulation results

A practical approach towards assessing the importance of the error term in any given case is to determine the fully converged real-space Madelung energy, forces, and stresses for various values of α; any change in the fully converged value with increasing α then signals the importance of including the error term. For example, according to Fig. 17 the fully converged Madelung energy of the perfect NaCl crystal is practically independent of α all the way up to $\alpha = 1.5/a$, as is the pressure (not shown), indicating that the error term is insignificant for this range of α values. This remarkable result demonstrates that, for $\alpha = 1.5/a$, a cutoff radius of $R_c = 1.5a$ is sufficient to accurately determine the Madelung constant, the reason being that the reciprocal-space term is only $\approx 2.0\times 10^{-6} q^2/a$ in this case (for details see Sec. VI C1).

The average energy and pressure per ion in molten MgO are shown in Figs. 18(a) and 18(b) for four values of α ranging between $0.8/a$ and $1.5/a$ (please note the highly expanded energy scale in comparison with Fig. 17). As discussed in Sec. III B, the melt was prepared by molecular-dynamics simulation using Buckingham-type interionic potentials[21] and a point-ion model in which the Coulomb energy, forces, and stresses were evaluated using the full 3D Ewald method. Two distinct effects of damping are clearly visible in Fig. 18. While increased damping significantly reduces the effective range of both the energy and pressure (from $R_c \approx 2.4a$ for $\alpha = 0.8/a$ to $R_c \approx 1.4a$ for $\alpha = 1.5/a$), the systematic errors thus introduced increase in a highly nonlinear fashion; interestingly, the errors in the energy and pressure are of comparable magnitude but have opposite signs. (For an analysis of this behavior, see Sec. VI C2.)

C. Discussion

In an attempt to better understand the magnitude and underlying physics of the error term at least for a 3D periodic system, we now analyze the $\mathbf{k=0}$ and $\mathbf{k\neq 0}$ contributions to

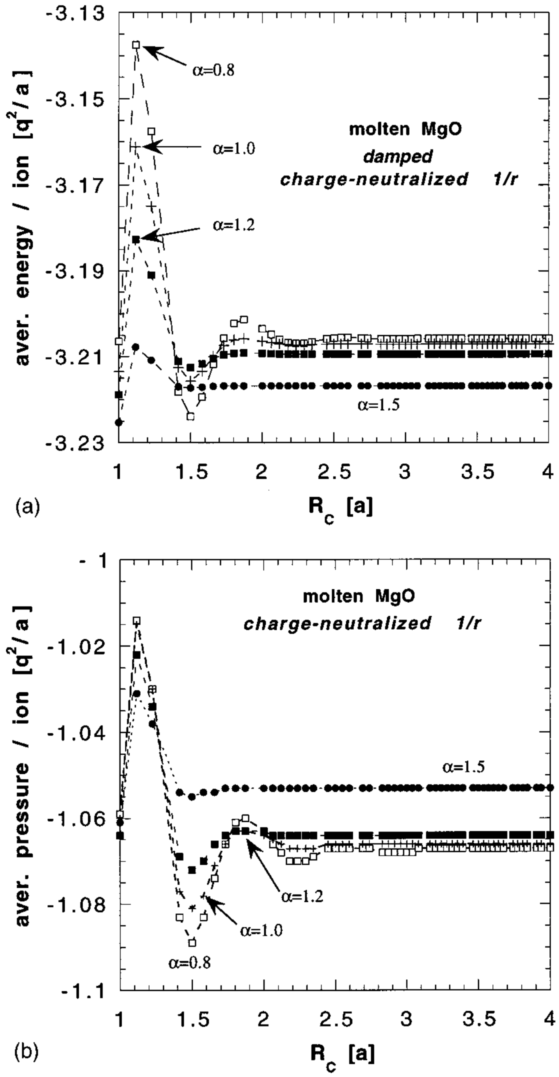

FIG. 18. Effect of damping in molten MgO on (a) the Madelung energy per ion and (b) the pressure per ion. Both are given in energy units of q^2/a; to convert the pressure (which is an energy *density*) into units of q^2/a^4, the data have to be divided by $3V$, where $V = a^3/8$ is the atomic volume [see also Eq. (5.23)].

$E_{\mathbf{k}}^{\mathrm{tot}}$ in Eq. (6.2). According to Eq. (6.3), the $\mathbf{k=0}$ damping correction vanishes unless the simulation cell has a net dipole moment. In many situations, a finite magnitude of $E^{(\mathbf{k=0})}$ arises from a finite-size effect introduced when 3D periodicity is imposed on an aperiodic system so as to enable the Fourier transformation. For example, an infinitely extended ionic melt will not, at any instant, exhibit a net dipole moment, by contrast with a finite-sized, periodically extended system. Including the $\mathbf{k=0}$ term, and the related forces and stresses, in the simulation would then give rise to the creation of a long-ranged dipole moment due to the artificially imposed periodicity; this in turn would systematically alter the dynamics of the infinite system and hence exacerbate this finite-size effect. In many cases the $\mathbf{k=0}$ term is therefore dropped from Eq. (6.2), thus more realistically representing the behavior of the infinite system. In all our simulations we have therefore omitted this term as well. For a 3D periodic system, Eq. (6.2) therefore simplifies as follows:

$$\Delta E_{\rm tot}^{\rm Mad} \equiv E_{(2)}^{\rm tot} \equiv E^{(\mathbf{k}\neq\mathbf{0})}. \tag{6.8}$$

The finite-**k** term in Eqs. (6.2) and (6.8) has a rather different physical origin than the $\mathbf{k}=\mathbf{0}$ term. According to Eq. (6.4), the term can be written as a $|\mathbf{k}|$-weighted sum over the peaks in the charge structure factor, $Q(\mathbf{k})$, defined in Eq. (4.18). Since, by definition, $Q(\mathbf{k})=|\sigma(\mathbf{k})|^2>0$, it follows that $E^{(\mathbf{k}\neq\mathbf{0})}>0$, i.e., in agreement with our simulations [see, e.g., Fig. 18(b)], the error term is always *positive*. This can be understood in terms of the definition of $E_{(2)}^{\rm tot}$ ($\equiv E^{(\mathbf{k}\neq\mathbf{0})}$) in Eq. (5.5): The self term [for $i=j$ in Eq. (5.5)] is always large and positive whereas all remaining terms are either positive or negative, their net effect being relatively small, i.e., $E_{(2)}^{\rm tot}>0$.

To illustrate the physical meaning of $E^{(\mathbf{k}\neq\mathbf{0})}$, we consider a crystalline system for which $Q(\mathbf{k})$ consists of a discrete set of Bragg peaks. As already discussed in Sec. IV B, the first peak in $Q(\mathbf{k})$ appears at $|\mathbf{k}_{\rm min}|\approx 2\pi/d(hkl)$ and is associated with the most widely spaced *charged* lattice planes, (hkl); all other Bragg peaks involve smaller spacings between charged lattice planes, and hence larger **k** vectors. By contrast with these **k** vectors, the **k** sum in Eq. (6.4) involves reciprocal-lattice vectors associated with the *simulation cell*, with its smallest values being of the order of $2\pi/L_\beta$, where L_β $(\beta=x,y,z)$ is the linear dimension of the simulation cell in the β direction.

Clearly, the magnitude of L_β has nothing to do with the physical length scale of the *material*. The essential physics of the finite-**k** term is therefore contained in the structural characteristics of the material as captured in $Q(\mathbf{k})$. The role of the prefactor of $Q(\mathbf{k})$ in Eq. (6.4) is therefore merely to weight this structure in $Q(\mathbf{k})$ in terms of an arbitrary length scale associated with the simulation cell. By assigning a particularly large weight to the lowest-**k** structural features, i.e., those with the longest wavelengths, $E^{(\mathbf{k}\neq\mathbf{0})}$ is a particularly sensitive function of structural features with a length scale of the simulation-cell size. As in the $\mathbf{k}=\mathbf{0}$ term, any system-size effects arising from the artificially imposed periodicity are therefore enhanced.

1. Zero-temperature perfect crystal

To establish a reference basis, we first analyze the error term for the perfect rocksalt crystal at zero temperature, with charges $\pm q$. Given that the {111} planes are the most widely spaced *charged* planes in this structure, the first peak in $Q(\mathbf{k})$ appears at $|\mathbf{k}_{111}|=2\pi/d(111)$ (see also Sec. IV B). Due to the perfect constructive interference for this **k** vector, Eq. (4.18) yields $Q(\mathbf{k}_{111})=N$, where N is the total number of ions in the simulation cell. According to Eq. (6.4), the related contribution to the error term from all eight equivalent [111] directions is given by

$$E^{(\mathbf{k}_{111})}=8\,\frac{2\pi N^2 q^2}{V}\,\frac{\exp(-|\mathbf{k}_{111}|^2/4\alpha^2)}{|\mathbf{k}_{111}|^2}. \tag{6.9}$$

For sufficiently small values of α this term dominates in $E^{(\mathbf{k}\neq\mathbf{0})}$ because the remaining peaks in $Q(\mathbf{k})$ are at larger **k** vectors and hence more severely damped by the exponential factor. With $d(111)=(\sqrt{3}/3)a$ and $V=Na^3/8$ for the NaCl lattice, Eq. (6.9) yields

$$E^{(\mathbf{k}_{111})}/N=\frac{32q^2}{3\pi a}\exp(-3\pi^2/\alpha^2 a^2). \tag{6.10}$$

For example, for $\alpha=1.0/a$ and $1.5/a$ this expression yields values of 4.7×10^{-13} and $2.0\times 10^{-6} q^2/a$, respectively, i.e., the term is negligible (see also Fig. 17). The same analysis can be applied to any perfect-crystal structure, leading to the conclusion that for $\alpha\leqslant 1.5/a$ the error term is totally negligible and for larger α values the term increases approximately exponentially as a function of α^{-2} [see Eq. (6.10)].

2. Effects of thermal disorder: High-temperature crystal and melt

The effect of thermal disorder in a perfect crystal is readily estimated. As a simple model we consider a crystal with randomly displaced ions, $\mathbf{r}_i=\mathbf{r}_i^0+\mathbf{u}_i$, where $\mathbf{r}_i^0$ indicates perfect-crystal lattice sites and the $\mathbf{u}_i$ are small displacement vectors ($|\mathbf{u}_i|\ll a$) relative to these sites. Insertion of these into Eq. (4.18) yields

$$Q(\mathbf{k})=\frac{1}{q^2N}\left|\sum_{i=1}^{N} q_j \exp[i(\mathbf{k}\cdot\mathbf{u}_i)]\exp[i(\mathbf{k}\cdot\mathbf{r}_i^0)]\right|^2. \tag{6.11}$$

As discussed earlier, provided α is small enough we need only evaluate $Q(\mathbf{k})$ for small **k** vectors where Eq. (6.11) simplifies as follows:

$$Q(\mathbf{k})\approx\frac{1}{q^2N}\left|\sum_{i=1}^{N} q_j(1+i\mathbf{k}\cdot\mathbf{u}_i)\exp(i\mathbf{k}\cdot\mathbf{r}_i^0)\right|^2$$
$$=\frac{1}{q^2N}\left|\sum_{i=1}^{N} q_j(\mathbf{k}\cdot\mathbf{u}_i)\exp(i\mathbf{k}\cdot\mathbf{r}_i^0)\right|^2. \tag{6.12}$$

Here we have used the fact that the perfect-crystal charge structure factor vanishes for small **k** vectors ($|\mathbf{k}|<|\mathbf{k}_{\rm min}|=|\mathbf{k}_{111}|$). Assuming uncorrelated, random displacements of the ions (i.e., ignoring any effects of phonons), the average of the dot product is simply given by $\langle\mathbf{u}_i\mathbf{u}_j\rangle=\langle u^2\rangle\delta_{ij}$. Equation (6.12) then becomes

$$Q(\mathbf{k})=\langle(\mathbf{k}\cdot\mathbf{u}_i)^2\rangle=\tfrac{1}{3}k^2\langle u^2\rangle, \tag{6.13}$$

where the factor of 1/3 comes from the directional averaging. Equation (6.4) then yields

$$E^{(\mathbf{k}\neq\mathbf{0})}\approx\frac{2\pi}{3V}Nq^2\langle u^2\rangle\sum_{\mathbf{k}\neq\mathbf{0}}^{\infty}\exp(-k^2/4\alpha^2). \tag{6.14}$$

Replacing the discrete sum by the integral, i.e., $\Sigma_{\mathbf{k}}\to V/(2\pi)^3\int d^3\mathbf{k}$ and using Eq. (4.16), this expression can be evaluated approximately to give

$$E^{(\mathbf{k}\neq\mathbf{0})}\approx\frac{1}{3\pi}Nq^2\langle u^2\rangle\int dk k^2\exp(-k^2/4\alpha^2)$$
$$\approx 0.38N\frac{q^2}{a}\frac{\langle u^2\rangle}{a^2}(\alpha a)^3. \tag{6.15}$$

To test the validity of this approximate expression, Fig. 19 shows the full error term determined directly for a perfect MgO crystal with randomly displaced ions for a range of α values; the average magnitude, $\langle u^2\rangle$, of the random displacements was chosen such as to correspond to $T=2500$ K in the

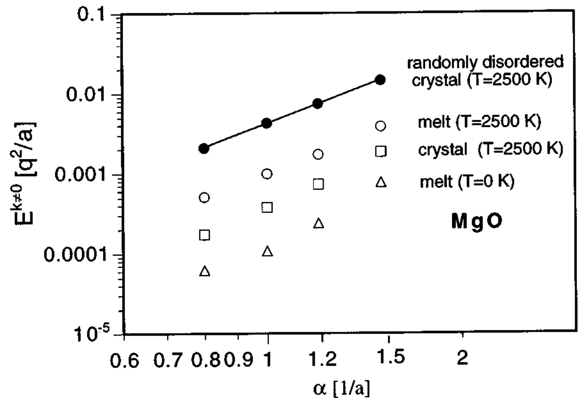

FIG. 19. Doubly logarithmic plot of the error term [Eq. (6.8)] vs α obtained from constant-pressure simulations for MgO using the full 3D Ewald sum. In agreement with Eq. (6.15) (solid line), the data calculated directly for the randomly disordered crystal (with $\langle u^2\rangle$ corresponding to the actual crystal at $T=2500$ K; closed circles) exhibit a slope of 3.0. Also shown are the results for the actual crystal at $T=2500$ K (in which the effects of phonons are fully incorporated), the supercooled melt at $T=2500$ K, and the melt quenched to $T=0$ K with subsequent relaxation of the ion positions and the pressure.

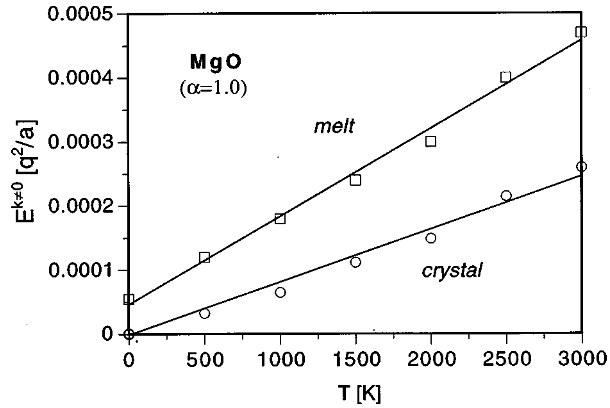

FIG. 20. Temperature dependence of the error term for molten MgO (squares) and the perfect crystal (circles) for $\alpha=1.0/a$. The solid lines represent linear fits to the data.

actual crystal determined by molecular-dynamics simulations using the full Ewald sum. According to Fig. 19, the agreement between these directly calculated values (closed circles) and the approximate results obtained from Eq. (6.15) for the same value of $\langle u^2\rangle$ is excellent (solid line, with a slope of 3.0). Therefore, the approximate expression (6.15), indeed, represents the small-α expansion of the error term for a randomly disordered perfect crystal.

Contrary to the assumption underlying Eqs. (6.13) and (6.14), in reality the ion movements are correlated due to the phonons. To analyze the effects of these correlations on the error term, we performed constant-pressure molecular-dynamics simulations for the perfect MgO crystal at $T=2500$ K using the full 3D Ewald sum (squares in Fig. 19). According to Fig. 19, these correlations reduce the error term by nearly an order of magnitude relative to the uncorrelated case (closed circles). Interestingly, however, the α^3 increase in $E^{(\mathbf{k}\neq\mathbf{0})}$ is practically unaffected by these correlations, suggesting that Eq. (6.15) remains approximately correct if we replace $\langle u^2\rangle$ by $\approx 0.1\langle u^2\rangle$. One reason for the dramatic reduction in $E^{(\mathbf{k}\neq\mathbf{0})}$ due to phonons is that most phonon branches are electrically inactive, i.e., they do not contribute to $Q(\mathbf{k})$.

It is well known that for crystalline systems the value of $\langle u^2\rangle$ is approximately proportional to the temperature and inversely proportional to the bulk modulus, B, i.e.,

$$\frac{\langle u^2\rangle}{a^2}\approx Ck_BT/B, \tag{6.16}$$

where k_B is the Boltzmann constant and C is a proportionality factor. (This expression is readily derived within a harmonic approximation in which the ions are connected to the perfect-crystal lattice by harmonic springs and all ions vibrate independently of each other.) Inserting Eq. (6.16) into Eq. (6.15) yields

$$E^{(\mathbf{k}\neq\mathbf{0})}/N=0.38C(\alpha a)^3\frac{q^2}{a}\frac{k_BT}{B}, \tag{6.17}$$

i.e., the error term for a crystal at finite temperature should increase approximately linearly with T. The molecular-dynamics simulation results in Fig. 20, obtained for a value of $\alpha=1.0/a$, demonstrate that this is, indeed, true not only for the crystal (circles) but also for the melt (squares). The lower density of the melt compared to the crystal results in a smaller bulk modulus; this is the reason for the higher slope in the linear fit to the data for the melt.

In contrast to the crystal, the melt exhibits two types of structural disorder, which we refer to as ''thermal disorder'' and ''coordination disorder.'' First, as in the crystal, the ions in the melt perform thermal vibrations with a magnitude similar to that in the crystal. Second, the melt is further disordered, as evidenced by the presence of coordination defects. These are responsible for the fact that, even upon elimination of the thermal disorder (e.g., by quenching to $T=0$ K with subsequent relaxation of the forces and the pressure), the error term for the melt has a finite value at $T=0$ K (see Fig. 20).

The contribution to $E^{(\mathbf{k}\neq\mathbf{0})}$ from the coordination disorder can be assumed to be roughly independent of temperature and given by its value at $T=0$ K. The strong, nearly tenfold increase in $E^{(\mathbf{k}\neq\mathbf{0})}$ in Fig. 20 with increasing temperature, from $\approx 0.5\times 10^{-4}q^2/a$ at $T=0$ K to $\approx 4.8\times 10^{-4}q^2/a$ at $T=3000$ K, is therefore almost entirely due to the thermal disorder. At elevated temperatures $E^{(\mathbf{k}\neq\mathbf{0})}$ for the melt is therefore dominated by the *thermal* disorder. For this reason, it is not surprising that both the high-temperature crystal and the melt are equally well described by the approximate expressions (6.15) and (6.17) (see Figs. 19 and 20).

Particularly interesting is the increase in $E^{(\mathbf{k}\neq\mathbf{0})}$ proportional to α^3, which arises from the fact that in the small-k limit,

$$Q(k)\approx Dk^2, \tag{6.18}$$

where D is a constant. This quadratic form is a general feature of any equilibrium ionic system (except the zero-temperature perfect crystal, which represents a special case). Equation (6.18) follows from the fact that, by definition,

$Q(k)$ is a symmetric function of k, i.e., $Q(k)=Q(-k)$ [see Eqs. (4.15) and (4.18)], and that charge neutrality requires that $Q(k=0)=0$.

To determine the related energy, $E^{(\mathbf{k}\neq\mathbf{0})}$, we replace the sum in Eq. (6.4) by the integral and use Eq. (4.16) to write

$$E^{(\mathbf{k}\neq\mathbf{0})}\approx\frac{Nq^2}{4\pi^2}\int d^3\mathbf{k}\,\frac{\exp(-k^2/4\alpha^2)}{k^2}Q(\mathbf{k})$$
$$=\frac{Nq^2}{\pi}\int dk\,\exp(-k^2/4\alpha^2)Q(k)\approx\frac{2Nq^2D}{\pi^{1/2}}\alpha^3, \tag{6.19}$$

where the last equality follows from insertion of Eq. (6.18), recognizing that this relation is valid only for sufficiently small values of α (see also Sec. VI C1).

Also starting from Eq. (6.4), the pressure associated with $E^{(\mathbf{k}\neq\mathbf{0})}$ can be evaluated following a similar procedure. Using the well-known trick of rescaling the ionic positions by $\mathbf{r}=V^{1/3}\mathbf{s}$ (where $\mathbf{s}$ represents ''reduced,'' volume-independent coordinates), this pressure can be written as follows:

$$p^{(\mathbf{k}\neq\mathbf{0})}=-\frac{\partial E^{(\mathbf{k}\neq\mathbf{0})}(V^{1/3}\mathbf{s})}{\partial V}$$
$$=\frac{2\pi Nq^2}{3V}\sum_{\mathbf{k}\neq\mathbf{0}}^{\infty}(1-k^2/2a^2)\frac{\exp(-k^2/4\alpha^2)}{k^2}Q(\mathbf{k}). \tag{6.20}$$

Then, following the same procedure as in the derivation of Eq. (6.19), the small-α expression for $p^{(\mathbf{k}\neq\mathbf{0})}$ becomes

$$p^{(\mathbf{k}\neq\mathbf{0})}=-\frac{4\rho q^2D}{\pi^{1/2}}\alpha^3, \tag{6.21}$$

where $\rho=N/V$ is the number density.

This result shows that $p^{(\mathbf{k}\neq\mathbf{0})}\sim\alpha^3$, i.e., like the systematic error in the real-space energy, the related error in the pressure can be made arbitrarily small by simply making α small. Remarkably, however, in the small-α limit $p^{(\mathbf{k}\neq\mathbf{0})}$ is always *negative* for an equilibrium ionic (solid or liquid) system; consistent with Fig. 18(b), this result indicates that damping of the real-space pair potential results in the loss of cohesion in the system.

For equilibrium ionic *liquids*, the constant D in Eqs. (6.18)–(6.21) can be evaluated using the Stillinger–Lovett second moment condition,[20] according to which

$$D=\lambda^2=\frac{k_BT}{4\pi\rho q^2}, \tag{6.22}$$

where λ is the Debye screening length. Insertion of Eq. (6.22) into Eqs. (6.19) and (6.21) yields

$$E^{(\mathbf{k}\neq\mathbf{0})}\approx\frac{Nk_BT}{2\rho\pi^{3/2}}\alpha^3, \tag{6.23}$$

$$p^{(\mathbf{k}\neq\mathbf{0})}\approx-\frac{k_BT}{3\pi^{3/2}}\alpha^3. \tag{6.24}$$

In the simulation of liquids, by simply adding these analytic expressions to the energy and pressure [Eqs. (5.17) and (5.23)], the systematic errors due to damping can be greatly reduced. For example, up to $\alpha=1.2/a$ about 80% of the errors in Figs. 18(a) and 18(b) can thus be eliminated; for larger α values the small-α expansions in Eqs. (6.23) and (6.24) become gradually less valid.

3. Effect of structural correlations

A comparison of the error term for a chemically disordered, structurally unrelaxed and relaxed perfect crystal at $T=0$ K is helpful for understanding why the contribution due to coordination disorder in the melt is much smaller than that due to thermal disorder. To generate a chemically disordered perfect crystal, the positive and negative nearest-neighbor charges on the NaCl lattice were randomly exchanged. The initial, unrelaxed structure then yields the relatively large value for $\Delta E_{\mathrm{tot}}^{\mathrm{Mad}}\equiv E^{(\mathbf{k}\neq\mathbf{0})}$ of about $0.08q^2/a$ (for $\alpha=1.0/a$); by contrast, in the fully relaxed system the error term of $\approx0.2\times10^{-3}$ is over two orders of magnitude smaller and of similar magnitude as that of the melt quenched to zero temperature.

This comparison suggests that thermal disorder is capable of generating higher-energy structural states that affect the related $Q(\mathbf{k})$ in a manner similar to the structural effects present in a not fully relaxed system. By localizing the coordination disorder, the effect of the relaxation of the ions is to greatly reduce long-range structural effects present in the unrelaxed $Q(\mathbf{k})$ while generating a physically realistic structure. Given the great sensitivity of the error term to such usually artificial and/or unphysical long-range effects, it is not surprising that its value drops dramatically upon relaxation. The reduction in the value of $E^{(\mathbf{k}\neq\mathbf{0})}$ in Fig. 19 by an order of magnitude when replacing the random displacements of the ions in the randomly disordered perfect crystal by the actual, highly correlated displacements in the high-temperature crystal represents another example of this simple principle. This principle is related to the simple notion of screening as given by the Poisson equation and the Boltzmann factor, i.e., charges obeying Poisson's equation tend to arrange in such a way as to screen their own Coulomb potential.

In summary, the magnitude of $E^{(\mathbf{k}\neq\mathbf{0})}$ depends strongly on the degree of *long-range* structural disorder in the system, particularly on whether or not the simulated system is in structural equilibrium and on long-range structural correlations associated with phonons. Due to structural features spanning the entire length of the simulation cell, an unrelaxed, highly disordered system may thus exhibit features in $Q(\mathbf{k})$ well below $|\mathbf{k}_{\mathrm{min}}|$; however, relaxation usually has the effect of localizing any structural disorder, and hence eliminating or greatly reducing these artificial, small-$|\mathbf{k}|$ structural features. Also, the effect of thermal disorder is to establish, via the phonons, medium- and long-range structural features appearing in the small-$|\mathbf{k}|$ regime in $Q(\mathbf{k})$, which hence contribute to the error term.

4. Range of the Madelung potential in liquids and solids

As for the molecular system and the undamped, charge-neutralized system, we now investigate the effective range of the Madelung potential obtained for the damped, shifted Coulomb pair potential [see Eqs. (5.7) and (5.13)]. According to Eq. (2.5), this requires determination of the energy of interaction of the ions with the material beyond R_c. Because of the damping in Eq. (5.13), this energy falls off exponentially with increasing R_c; its value for a given value of R_c is controlled by erfc(αR_c) [see Eq. (5.13)]. The *exponentially short* range of the Madelung potential thus obtained is based solely on the contribution to $V_{\text{eff}}(r)$ in Eq. (2.5) from the *real-space* Madelung energy in Eq. (5.7); it ignores possible *long-range* effects that might arise from the *reciprocal-space* term and hence control the actual range of the potential.

According to Eq. (6.8), the reciprocal-space energy represents the systematic error, $E_{(2)}^{\text{tot}} \equiv E^{(\mathbf{k}\neq\mathbf{0})}$, introduced by the damping; this energy has to be incorporated into $V_{\text{eff}}(r)$ in order to obtain the effective range of the total Madelung energy from Eq. (2.5). Equation (6.8), connecting the α-dependent reciprocal-space quantity $E^{(\mathbf{k}\neq\mathbf{0})}$ with the real-space quantity $E_{(2)}^{\text{tot}}$, permits the effective range of the reciprocal-space Madelung potential to be estimated. Because of the error function, the individual contributions, $q_i q_j \,\text{erf}(\alpha r_{ij})/r_{ij}$, to $E_{(2)}^{\text{tot}}$ in Eq. (5.5) differ significantly from zero only when $\alpha r_{ij} \gtrsim 1$, showing that $E^{(\mathbf{k}\neq\mathbf{0})}$ can be interpreted as representing the energy of interaction of some average ion with all the ions located beyond some cutoff distance, $R_c \sim 1/\alpha$. The α^3 variation of $E^{(\mathbf{k}\neq\mathbf{0})}$ described by Eq. (6.19) therefore implies that $E_{(2)}^{\text{tot}} \sim D R_c^{-3}$; this range is considerably longer than that associated with the *exponentially* short-ranged real-space energy.

The rather short R_c^{-3} effective range of the Madelung energy[16] of any equilibrium ionic system, which corresponds to $V_{\text{eff}}(r) \sim D r^{-6}$ [see Eq. (2.5)], is striking in that it is exactly the same as that of the Lennard-Jones potential (see Sec. II B). Analysis of the interaction-strength parameter, D, can provide insight into the origin of this r^{-6} decrease of $V_{\text{eff}}(r)$. Starting from Eq. (6.18), D can be calculated from the expression

$$D = \frac{1}{2} \left. \frac{\partial^2 Q(k)}{\partial k^2} \right|_{k=0}. \tag{6.25}$$

Then, combining the definition of $Q(k)$ in Eqs. (4.15) and (4.18) with the charge-neutrality condition, it is straightforward to show that D represents the following ensemble average:

$$D \sim \int\int d^3\mathbf{r} d^3\mathbf{r}' \,\mathbf{r}\sigma(\mathbf{r})\mathbf{r}'\sigma(\mathbf{r}') = \int\int d^3\mathbf{r} d^3\mathbf{r}' \,\mathbf{p}(\mathbf{r})\mathbf{p}(\mathbf{r}'), \tag{6.26}$$

where $\mathbf{p}(\mathbf{r}) = \mathbf{r}\sigma(\mathbf{r})$ is the local dipole moment. Unless the system is polarized, in thermodynamic equilibrium these local dipoles fluctuate about zero. The dipole–dipole correlation function in Eq. (6.26) therefore describes the coupling between fluctuating local dipoles. As is well known, this type of coupling has the r^{-6} range of van der Waals interactions and constitutes the physical justification for the attractive part of the Lennard-Jones potential.

We finally mention that a perfect-crystal lattice represents an exception to the general R_c^{-3} behavior since it is easy to group the ions in such a way as to avoid any local dipoles. As discussed in Sec. VI C1, $Q(k)$ then vanishes identically between $k=0$ and the first crystalline peak, resulting in Eq. (6.9) for $E^{(\mathbf{k}\neq\mathbf{0})}$. Substituting α by $1/R_c$, $E_{(2)}^{\text{tot}} \equiv E^{(\mathbf{k}\neq\mathbf{0})}$ is readily seen to decrease exponentially with R_c. As a consequence $V_{\text{eff}}(r)$ [see Eq. (2.5)] falls off faster than any inverse power of r. However, even a small perturbation of the perfect lattice sites generates local dipoles, yielding $V_{\text{eff}}(r) \sim r^{-6}$.

TABLE I. Combinations of the damping parameter, α, and truncation radius, R_c, for the charge-neutralized, damped r^{-1} Coulomb sum used in our molecular-dynamics simulations of MgO. The value of R_c for a given choice of α was chosen such that the pressure in the zero-temperature perfect crystal is practically converged. For comparison, the parameters used for the spherically truncated, fully converged 3D Ewald sum are also listed. For the MgO interionic potentials of Sangster and Stoneham (Ref. 21), the Ewald sum gives a zero-temperature lattice parameter of $a_0 = 4.2271$ Å.

	$\alpha(a_0^{-1})$	$R_c(a_0)$
Damped r^{-1}	1.0	2.71
Damped r^{-1}	1.2	2.00
Damped r^{-1}	1.5	1.46
Full Ewald	2.5	1.5

VII. MOLECULAR DYNAMICS SIMULATIONS

The simulations of bulk and interfacial systems reported so far in this article involved the full Ewald sum, 3D periodic, or Parry's slab version,[25] against which the directly summed, r^{-1} Coulomb energy, forces, and stresses could be tested. In the following we discuss a few molecular-dynamics simulations which, by contrast, directly apply the above method by utilizing the charge-neutralized, damped r^{-1} pair potential in Eq. (5.11) and the related forces and stresses given by Eqs. (5.21)–(5.23). Since, by virtue of the charge-neutrality condition, the pair potential and all its derivatives are smoothly shifted to zero at R_c, these expressions are well suited to provide the basis for molecular-dynamics simulations. Using the combinations of the damping parameter, α, and truncation radius, R_c, listed in Table I, these simulations can be compared directly with simulations involving the full Ewald sum.

In the following we consider a 3D periodic, perfect MgO crystal in a cubic simulation cell of size $(6a)^3$ containing 432 MgO molecules described by the interionic potentials of Sangster and Stoneham.[21] The crystal is gradually heated, under zero external pressure, through the melting transition while the lattice parameter, atomic structure, mean-square displacements, and internal energy are monitored.

In principle, a system described by Eqs. (5.11) and (5.21)–(5.23) need not conserve energy because the energy does not quite represent the correct integral of the forces (see also Sec. III D). Although the energy and its derivatives are therefore not entirely consistent with one another, the shifting method in Eqs. (3.24) and (5.11) based on the concept of charge neutralization has the advantage that the actual values for the energy, forces, and pressure thus obtained are as close as desired to the correct ones, i.e., to those obtained for the unshifted potential. Therefore, as a critical test of our simulation method, we carefully investigated the degree to which, in microcanonical-ensemble simulations, the condition of energy conservation is satisfied.

As a test of the numerical consistency of the energy and forces, we performed constant-volume simulations of the crystal for $\alpha = 1.5/a_0$, $R_c = 1.46a_0$ (the most strongly damped, and hence shortest-range case; see Table I) for two different time steps: $\Delta t = 0.43$ and 2.15 fs; a_0 is the zero-temperature lattice parameter. For the shorter time step, at a mean temperature of ~900 K and over a simulation time of 4.3 ps the energy fluctuated about the mean value of -40.517 eV/molecule by ~0.001 eV/molecule; a fluctuation by this amount in the kinetic energy of a molecule translates into a fluctuation in the temperature of only ~4 K, which is perfectly acceptable. For the longer time step, we observed in addition a small upward drift of the energy of ~0.0005 eV/molecule/ps.

To separate the limitations inherent to the direct-summation method from those arising from the numerical integration of the equations of motion, we compared the above results with those obtained for the full Ewald method, for which all departures from exact energy conservation are entirely due to the numerical integration scheme. The fluctuations in the energy are then only ~0.000 01 eV/molecule for the shorter time step while for the longer time step a small upward drift of 0.0007 eV/molecule/ps is observed. This comparison indicates that the small drift is due to the finite time step in the integration scheme and not the direct-summation method. Thus, although, as anticipated, the energy fluctuations are considerably larger for the direct-summation method than for the full Ewald method, they are still rather small on an absolute scale. These differences are entirely irrelevant when the temperature is rescaled during the simulation.

Given these results, the longer of the two time steps combined with energy rescaling was used to (i) heat the perfect MgO crystal above the melting point, T_m (estimated at ~3200 K for our potential) and (ii) cool the melt below T_m. In Figs. 21(a) and 21(b) the temperature dependence of the lattice parameter, $a(T)$, and internal energy are compared for the four sets of parameters in Table I. Clearly, the discontinuity in both quantities between 3000 and 3500 K is due to the melting transition; the superheating of the crystal and the supercooling of the melt is due to the fact that the defect-free perfect crystal contains no nucleation centers, such as dislocations or free surfaces, that could trigger the first-order transition between the two phases at the melting point.[33]

According to Figs. 21(a) and 21(b), the four parameter sets give rather similar results, although at the highest temperatures the melt clearly exhibits a lower density for the largest value of α. Following the discussion in Sec. VI C2, in this regime the error term increases rapidly with increasing values of α and with temperature (see Figs. 19 and 20). For more accurate simulations in this regime, it would therefore be advisable to apply less damping (i.e., choose a smaller α value), with a consequently larger cutoff radius. As a more efficient alternative, one could simply compensate for the systematic errors due to damping made in the real-space

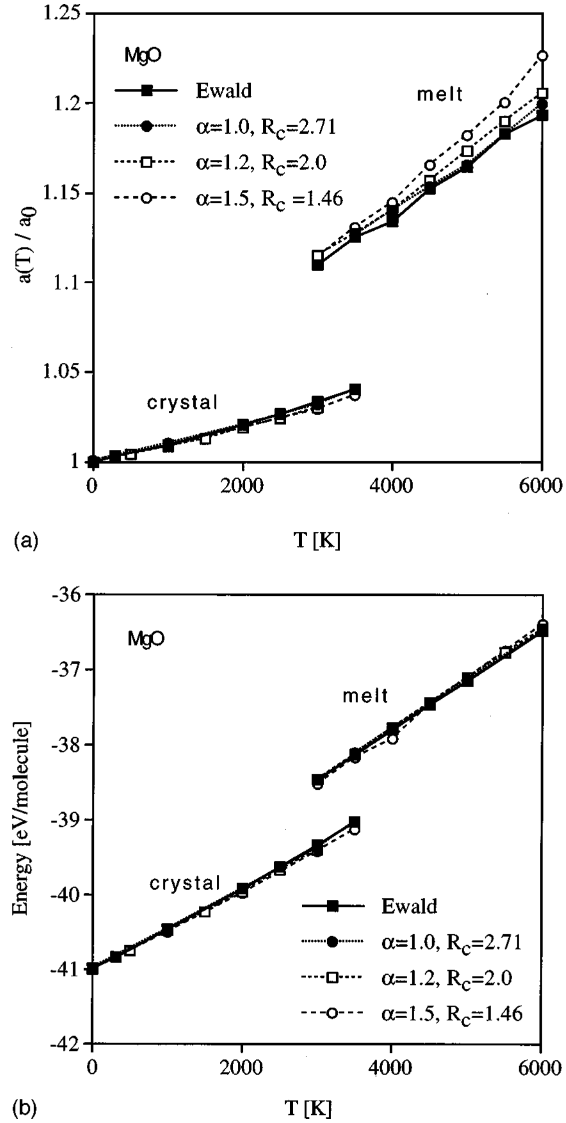

FIG. 21. Temperature dependence of (a) the lattice parameter (in units of a_0) and (b) the internal energy per ion for the four sets of parameters in Table I.

pressure and energy. This requires adding $p^{(\mathbf{k}\neq 0)}$ and $E^{(\mathbf{k}\neq 0)}$ given by Eqs. (6.24) and (6.23) to Eqs. (5.23) and (5.17), respectively. For example, the additional cohesion provided by $p^{(\mathbf{k}\neq 0)}$ will increase the density of the melt, thus greatly reducing the systematic errors in the thermal expansion in Fig. 21(a).

To investigate how damping affects other properties of the melt, we have also determined the structure and self-diffusion behavior. As described in Sec. IV A, in ionic systems two structural measures are equally useful, the radial distribution function, $G(r)$, and the radial charge distribution function, $Q(r)$ [see Eqs. (4.1) and (4.2)]. In Fig. 22, $G(r)$ and $Q(r)$ at 6000 K obtained for the four sets of simulation parameters are compared. According to these results, in spite of the slightly different densities [see Fig. 21(a)], the differences among the four parameter sets are remarkably small in both $G(r)$ and $Q(r)$, suggesting that even for the strongest damping ($\alpha = 1.5/a_0$) the distribution of the atoms and charges in the melt is reproduced very well. Given Eqs. (4.1)

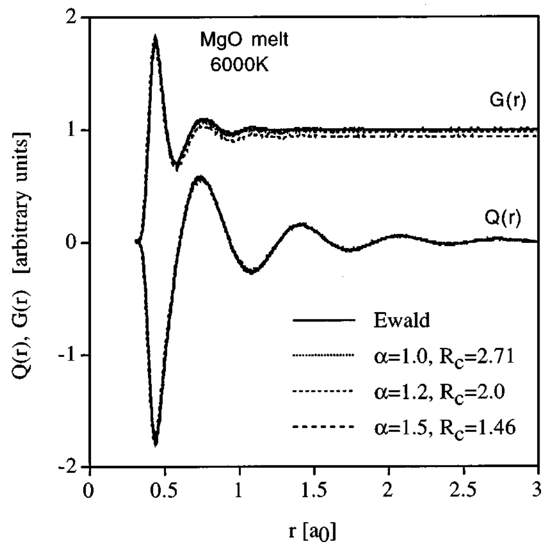

FIG. 22. $G(r)$ and $Q(r)$ [see Eqs. (4.1) and (4.2)] for molten MgO at 6000 K for the four sets of parameters in Table I.

and (4.2), we conclude that the underlying partial radial distribution functions differ by equally little, i.e., the underlying atomic structure of the melt is a rather insensitive function of α and R_c. This behavior is consistent with the large body of simulations of ionic melts in which it was found that omission of the reciprocal-space term in the Ewald sum has practically no effect on the structure of the melt.[6,7]

In the Arrhenius plot in Fig. 23 the mean-square displacements of the ions in the melt are plotted against the reciprocal temperature between 3000 and 6000 K. The activation energy obtained from least-squares fits to the four data sets increases from 0.96 eV/ion for the full Ewald sum to 1.04 eV for the strongest damping. As for the density of the melt [Fig. 21(a)], this comparison suggests that for more precise simulations in this regime, less damping should be applied; alternatively, the systematic errors due to damping can be greatly reduced by incorporating Eqs. (6.23) and (6.24) into the simulation.

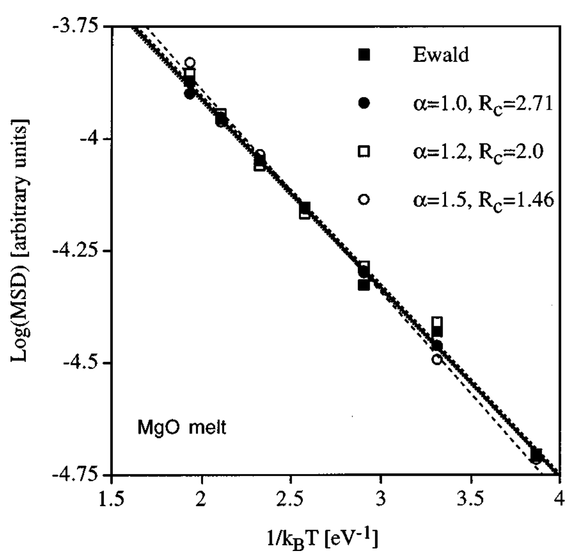

FIG. 23. Arrhenius plot for the mean-square displacement of the ions in the melt vs reciprocal temperature between 3000 and 6000 K for the four sets of parameters.

In summary, the above results demonstrate that even relatively strong damping combined with a very short cutoff radius reproduces the structure and properties of the crystal and the melt remarkably well. Also, as expected from our analysis of the error term, by simply reducing the degree of damping combined with an increase in the cutoff radius, the Ewald limit can be approached with arbitrary precision.

VIII. SUMMARY AND CONCLUSIONS

In this article we have described an exact method for the simulation of Coulombic systems by spherically truncated, pairwise $1/r$ summation. At the outset we observed that the problems encountered when performing a spherically truncated pairwise r^{-1} sum in a crystal or liquid are a direct consequence of the fact that, wherever one truncates, the system summed over is practically never neutral. Our method is based on recent work showing that the Coulomb potential in an arbitrarily disordered, condensed ionic system is short ranged. In this work, local charge neutrality is achieved by viewing an ionic crystal as a molecular system consisting of Bravais lattice sites on which complete molecules are placed, with the proviso that molecules may not be broken up so as to preserve charge neutrality.[11,12] This method contains Evjen's approach[4] as a special case.[11,12]

The key achievement in this article is the mapping of a spherically truncated, generally charged local environment of the ions onto this molecular picture. This mapping demonstrates that any net charge in the local, spherical environments of the ions arises from the breaking up of molecules situated near the surface of the truncation sphere of each ion. In zeroth order, these charges may be thought of as sitting *exactly at* the surface of the truncation sphere. The result is a simple expression for neutralizing the net charge in the truncation sphere of each ion, thus enabling the extraction of the Coulomb energy, forces, and stresses from the spherically truncated environment in a straightforward, physically transparent manner.

An interesting computational aspect of the method is that the physical concept of charge neutralization at the system surface is mathematically equivalent to the operational concept of shifting the pair potential to zero at the cutoff radius. The charge-neutralized potential of the spherically truncated system and all its derivatives therefore approach zero smoothly at R_c. Spherical truncation with charge neutralization also eliminates the net dipole moment in the ''molecular'' system. However, in spite of this avoidance of a macroscopic polarization, the neutral local environments of the ions exhibit fluctuating dipoles which determine the effective range of the net Coulomb potential.

Our convergence analysis revealed that the energy of the charge-neutralized system approaches the correct Madelung energy in a damped, oscillatory manner, demonstrating that the concepts of charge neutralization and damping are intricately connected. This leads us naturally to the operational approach of simply damping the Coulomb pair potential so as to flatten out these already damped symmetric oscillations even faster. The practical challenge with this approach is to assess the systematic errors in the energy, forces, and stresses thus introduced for any assumed form of the damping function.

If we assume a damping function given by the complementary error function, the above method offers a simple physical interpretation of the Ewald method: Whereas the real-space term in the Ewald sum gives the energy associated with the damped, *charged* (i.e., unshifted) pair potential, the less well understood reciprocal-space term represents the systematic error due to the damping. Interestingly, while this error term can alter the values towards which the real-space potential and its derivatives converge, it further reduces the already short range of the undamped Coulomb potential.

A detailed analysis of the reciprocal-space term has enabled us to show that the effective range of the Madelung potential in a high-temperature solid or a liquid is identical to that of the Lennard-Jones potential. Analogous to the van der Waals potential, this r^{-6} variation of the effective Madelung potential arises from the interaction between fluctuating dipoles present in any ionic equilibrium system.

Computationally our method is convenient and highly efficient. In particular, like the fast-multipole methods,[8–10] the computational load increases as order N. Unfortunately, however, it is difficult to make a precise comparison between them because of the number of parameters that can be varied to optimize the performance: α and R_c for the direct summation, the highest order multipole included, and the volumes over which the multipoles are averaged in the fast-multipole methods. Nevertheless, since for any given system the two methods must both describe the same physics and since both are of order N, their computational loads should not differ fundamentally for any given level of precision; one should keep in mind, however, that the prefactors in the two approaches are not the same.

Because of the spherical truncation and fast convergence, any standard computer code developed for handling pair potentials can be used to evaluate the Coulomb energy of an arbitrarily disordered, charged or neutral ionic system. Moreover, the underlying highly localized nature of the Coulomb potential, which translates into rather short cutoff radii, enables the use of a standard link-cell list,[26] demonstrating that our method is, indeed, an order-N method in both CPU time and memory, although a standard neighbor list approach can be used as well. This degree of simplicity has long been sought for Coulombic systems. A shifted ''spherical Ewald truncation'' was considered by Linse and Anderson[34] with limited success. Missing from their treatment were the creation of a charge-neutralized truncation sphere and the isolation of dominant contributions to the pair potential described here.

Our method is particularly powerful for the simulation of interfacial systems, such as bicrystals, free surfaces, and liquid–vapor interfaces. Because of the absence of periodicity in the direction normal to the interface, simulations of such systems require the use of Parry's extension of the 3D Ewald sum appropriate for a slab geometry.[25] Unfortunately, in contrast with the 3D Ewald sum, the reciprocal-space term in Parry's solution cannot be reduced to a single sum. Apart from the considerably greater mathematical complexity of Parry's expressions, the fact that these double sums have to be explicitly evaluated is prohibitively expensive; very few molecular-dynamics simulations of interfacial systems in a slab geometry have therefore been reported to date.[35] On the other hand, application of the 3D Ewald sum to such highly inhomogeneous systems can give rise to long-range interactions, absent in the real system, between the two interfaces artificially introduced into the simulation cell. None of these problems arises in our direct r^{-1} summation method for interfacial systems; thereby it offers a unique tool by which to investigate interfacial phenomena, such as screening and space-charge effects at individual interfaces.

ACKNOWLEDGMENTS

The authors have benefited from discussions with Robert Kulver. They are indebted to Markus Deserno from the Max-Planck Institute for Polymer Research in Mainz for many helpful suggestions on the manuscript. This work was supported by the U.S. Department of Energy, BES–Materials Science under Contract No. W-31-109-Eng-38.

[1] E. Madelung, Phys. Z. **19**, 524 (1918).
[2] P. P. Ewald, Ann. Phys. (Leipzig) **64**, 253 (1921).
[3] J. P. Hansen and I. R. McDonald, Phys. Rev. A **11**, 2111 (1975).
[4] H. M. Evjen, Phys. Rev. **39**, 675 (1932); see also, C. Kittel, *Introduction to Solid State Physics*, 3rd ed. (Wiley, New York, 1967), pp. 94–96.
[5] J. H. R. Clarke, W. Smith, and L. V. Woodcock, J. Chem. Phys. **84**, 2230 (1984).
[6] L. V. Woodcock, *Advances in Molten Salt Chemistry*, edited by J. Braunstein, G. Mamantov, and G. P. Smith (Plenum, New York, 1975), Vol. 3, p. 1.
[7] D. Fincham, Mol. Simul. **13**, 1 (1994).
[8] L. Greengard and V. Rokhlin, J. Comput. Phys. **73**, 325 (1987).
[9] L. Greengard, Science **265**, 909 (1994).
[10] H. Y. Wang and R. LeSar, J. Chem. Phys. **104**, 4173 (1996).
[11] D. Wolf, Phys. Rev. Lett. **68**, 3315 (1992).
[12] D. Wolf, Springer Proc. Phys. **80**, 57 (1995).
[13] F. Rohr, K. Wirth, J. Libuda, D. Cappus, M. Baumer, and H.-J. Freund, Surf. Sci. **315**, L977 (1994).
[14] D. J. Adams, Chem. Phys. Lett. **62**, 329 (1979); J. Chem. Phys. **78**, 2585 (1983).
[15] S. W. de Leeuw, J. W. Perram, and E. R. Smith, Proc. R. Soc. London, Ser. A **373**, 27 (1980).
[16] Although the terms ''Madelung energy'' and ''Madelung potential'' are usually associated with crystalline structures at zero temperature, here we use the terms more broadly in the sense of the R_c-dependent ''true'' Coulomb energy or potential of a given system (crystal, liquid, plasma, etc.).
[17] See, for example, J. D. Jackson, *Classical Electrodynamics*, 2nd ed. (Wiley, New York, 1975).
[18] R. Lacman, Colloq. Int. Centre Natl. Rech. Sci. (Paris) **152**, 195 (1965).
[19] J. Eggebrecht and D. Wolf (unpublished work).
[20] F. H. Stillinger and R. Lovett, J. Chem. Phys. **49**, 1991 (1968).
[21] M. J. L. Sangster and A. M. Stoneham, Philos. Mag. B **52**, 717 (1985).
[22] D. Wolf, J. Am. Ceram. Soc. **67**, 1 (1984).
[23] P. W. Tasker and D. M. Duffy, Surf. Sci. **137**, 91 (1984).
[24] D. M. Duffy and P. W. Tasker, Philos. Mag. A **47**, 817 (1983).
[25] D. E. Parry, Surf. Sci. **49**, 433 (1975); *ibid.* **54**, 195 (1975).
[26] M. P. Allen and D. J. Tildesley, *Computer Simulation of Liquids* (Clarendon, Oxford, 1987).
[27] H. L. Friedman, Mol. Phys. **29**, 1533 (1975).
[28] See, for example, B. E. Warren, *X-ray Diffraction* (Dover, New York, 1990).

[29] O. Emersleben, Math. Nachr. **4**, 468 (1951).
[30] D. Borwein, J. M. Borwein, and K. F. Taylor, J. Math. Phys. **26**, 2999 (1985).
[31] See, for example, N. H. March and M. P. Tosi, *Coulomb Liquids* (Academic, New York, 1984), p. 15.
[32] D. M. Heyes, J. Chem. Phys. **74**, 1924 (1981).
[33] S. R. Phillpot, S. Yip, and D. Wolf, Comput. Phys. **3**, 20 (1989); Phys. Rev. B **40**, 2831 (1988); **40**, 2841 (1988).
[34] P. Linse and H. C. Andersen, J. Chem. Phys. **85**, 3027 (1986).
[35] See, for example, D. M. Heyes and J. H. R. Clarke, J. Chem. Soc., Faraday Trans. 2 **77**, 1089 (1981); J. N. Gossli and M. R. Philpott, Electrochim. Acta **41**, 2145 (1996).